Numerical Modelling of LOX Droplet Combustion in Hydrogen under Micro-gravity Conditions

Sai Phani Keerthan Ponduri

A dissertation
submitted in partial fulfillment of the
requirements for the degree of

Master of Science

in

Aeronautics & **Astronautics**

University of Washington

2023

Graduate Committee:

Prof. James Hermanson, Chair

Prof. Owen Williams

Program Authorized to Offer Degree:
Aeronautics and Astronautics

University of Washington

Abstract

Numerical Modelling of LOX Droplet Combustion in Hydrogen under Micro-gravity Conditions

Sai Phani Keerthan Ponduri

Chair of the Supervisory Committee:
Prof. James Hermanson
Aeronautics and Astronautics

One of the most frequent liquid rocket propellant configurations is LOX/LH_2. Specifically, since this fuel/oxidizer mixture produces an extremely high specific impulse (Isp) with only water vapor as an exhaust. This makes LOX combustion research critical for improving combustion efficiency and avoiding flame instabilities in the rocket engine's combustion chamber. The spray dispersion method is used to inject liquid oxygen into the combustion chamber, whereas hydrogen enters the combustion chamber in a gas phase, as it is most likely to be pre-vaporized due to the regenerative cooling in the rocket nozzle. When the LOX droplets ignite, combustion happens between them and the surrounding hydrogen fuel environment.

The essential building block of this process is considered for this study, which is a single LOX droplet with a surrounding hydrogen environment, in order to analyze this physical process in an optimum fashion. This study assumes a micro-gravity environment as it slows down the process and allows for large droplets to be considered which facilitates better analysis of the phenomenon. It enables radially symmetrical domains. As a result, this problem is modeled in spherically symmetric co-ordinates using OpenFOAM. To model counter-flow combustion with 6-step oxygen/hydrogen

reactions, the reactingFoam solver from the OpenFOAM library is employed. A modified version of this reactingFoam solver names 'EBI-DNS', developed by a team at KIT, Germany, is also considered in this study which includes variable binary diffusion coefficients. The new solver considers the non-unity Lewis number constraint for each species required for this laminar combustion involving 100% hydrogen concentration.

The new solution predicts flame temperatures more accurately than the traditional reactingFoam solver, which produces incorrect flame temperatures when using 100% pure hydrogen as the fuel. A droplet vaporization model developed by the team at ZARM is considered in this study to match the gaseous phase flame modelling in OpenFOAM with liquid droplet evaporation. The rate of heat transfer at the droplet is studied in both cases to couple them as a single numerical solution of droplet combustion. Radiation heat transfer is also considered, as an addition to the flame model to match the rate of heat transfer for droplet evaporation obtained in experimentation.

The new EBI-DNS solver predicts flame temperatures close to 3100 K, which is quite similar to theoretical models' predictions of adiabatic flame temperatures. The outcomes provide a reasonable flame solution that can be tested using the experimental rate of heat transfer to the LOX droplet. The droplet model has been observed to not work for practical conditions of a surrounding temperature of about 3000K. Modelling conditions possible for radiation heat transfer such as black-body radiation, optically thin/thick assumption, and emissivities of the flame are proposed in this study. With a seemingly successful flame solution, and proposed additions to the model, this study contributes immensely to the ways in which a complete numerical solution to the LOX droplet combustion can be developed.

TABLE OF CONTENTS

LIST OF FIGURES

LIST OF TABLES

ACKNOWLEDGMENTS

I would first like to thank Prof. James C. Hermanson for his constant support as my graduate advisor and research mentor in guiding me through the research, helping me, motivating me, and suggesting detailed edits to the draft of this thesis. It was a great learning experience to work with him.

A special appreciation for our collaborators, Dr. Florian Meyer and Dr. Christian Eigenbrod, at ZARM, Germany, for their constant support and contribution to this study. I also wish to express my gratitude to Dr. Thorsten Zirwes and team as well, as our partners at KIT, for their invaluable contribution to this project by providing an important tool.

I would also like to thank Prof. Owen Williams for accepting my request to be on my Thesis committee and providing valuable suggestions and edits to this thesis. I would also like to thank him for introducing me to the research and working environment here at the University of Washington.

A special mention to the members of the Hermanson research group, Andrew Jansen, Mikael Godfrey, Andrew Jacobs, Jevoni Sykes, and Evelyn Madewell for their supportive group environment during this research.

I would also like to express my sincere appreciation to the University of Washington and the Department of Aeronautics and Astronautics, where I had the opportunity to work on this research as a part of my Master's Thesis.

Finally, I would like to show my extreme gratitude and love for my Parents, Family, and Friends everywhere for their long-lasting support, encouragement, and motivation.

Chapter 1
INTRODUCTION

1.1 Liquid Rocket Propulsion

Rocket Propulsion is a highly researched concept today with exponential growths of space exploration technologies in the past 50 years. Liquid rocket propulsion is a technology that uses liquid fuels and oxidizers to generate thrust for rocket engines. The use of liquid propellants provides high energy density, which allows for greater efficiency in space missions. Liquid rockets are commonly used in space exploration, satellite launching, and missile defense systems. The liquid rocket engine is one of the most common rocket propulsion systems in use currently. These engines enjoy performance advantages over solid motors. Most of the liquid rocket engines for bigger rockets employ a system of propellants called bipropellant, in which fuel and oxidizer are stored in separate tanks and then combined in the thrust chamber. These bipropellant systems provide a very high specific impulse as compared to monopropellant thrusters. The performance of the system also depends on the choice of propellants, which is why it is a very important design configuration for liquid rocket systems.

1.1.1 Choice of Propellants

Liquid Propellants employed in rockets are of three types: petroleum, cryogenic, and hypergolic or storable. This work is focused on cryogenic propellants, given that they are also one of the most commonly used ones today. Cryogenic propellants are liquified gases at extremely low temperatures. As the bi-propellant system employs both oxidizer and fuel as liquids in separate tanks, there is a need to select a cryogenic oxidizer along with the fuel. This combination is chosen as per the performance

required. Hence, liquid oxygen (LOX) and liquid hydrogen (LH_2) is one of the most commonly used sets of cryogenic oxidizer and fuel because of their high specific impulse and simple exhaust composition (water vapor). This system is also the focus of this study.

1.1.2 Method of dispersion

The cryogenic oxidizer and fuel are delivered to the thrust chamber through injectors. Because of the temperatures and regenerative cooling of the rocket nozzle, hydrogen vaporizes before entering the thrust chamber and typically exists as a gas during combustion. Oxygen on the other hand enters the thrust chamber in the form of droplets in a spray coming through the injector. These droplets interact with the hydrogen gas and after the ignition, the combustion occurs on the set of liquid oxygen droplets with a hydrogen gas environment around them.

1.2 Motivation

Optimizing the process of combustion to obtain an efficient rocket engine design requires a detailed analysis and study of the spray combustion process of liquid propellants that are mentioned in the previous section. The entire spray dispersion and combustion process is complicated with multiple super-positions and non-linearly coupled interactions of individual sub-processes. These include steps such as liquid jet disruption, atomization, droplet formation, vaporization, ignition, and combustion. Each of the sub-processes is complicated so the entire spray combustion process has not been modelled entirely accurately even in supercomputers. So it is important to break down this phenomenon into simple individual processes and study it in an ideal way initially. Hence, a single completely formed droplet in a radially symmetric hydrogen environment has been considered to study the combustion of a single liquid oxygen droplet in the hydrogen environment.

1.2.1 ZARM drop tower experiment

While some prior studies have been conducted on single LOX droplet vaporization under sub-critical and supercritical conditions in a quiescent or convective H_2 environment, few numerical models have been developed and validated with experimental data to completely understand the combustion behavior of the *LOX* droplet. This study aims to address this research problem, of developing a numerical model and validate it with experimental data of *LOX* evaporation and combustion. Our collaborators at ZARM, Germany, have developed a drop tower experiment in the facility at the University of Bremen, Bremen, Germany. These drop tower tests are conducted in micro-gravity conditions, in order to consider an ideal spherical droplet. The drop tower offers a micro-gravity quality of 10^{-6} g for a test duration of 4.9 s.

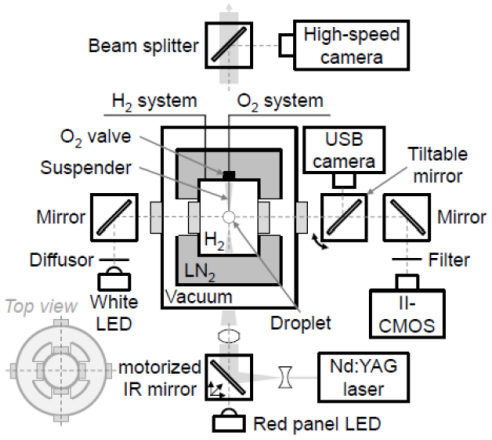

Figure 1.1: Schematic of the experimental setup for the combustion chamber diagnostics

Figure 1.1 shows the experimental setup and various diagnostic systems used to study the *LOX* droplet combustion. The setup consists of a combustion chamber containing the *LOX* droplet and H_2 gas surrounded by the liquid-nitrogen cooling jacket, which is then surrounded by a vacuum container that provides the necessary

thermal isolation. The combustion chamber is cooled to a fixed temperature of 77 K and the combustion chamber is connected to a gaseous supply of pure H_2. The liquid oxygen droplet enters the suspender tip within the combustion through a valve mounted on the top of the combustion chamber. The droplet is ignited within the combustion chamber through the pulsed Nd:YaG laser [5].

At the ZARM facility, 16 drop-tower tests in the pressure range of 1-45 bar have been completed thus far. All experiments were conducted in a 100% H_2 atmosphere. The experiment yielded a droplet lifetime estimate of 136.5 ms for a droplet of $700\mu m$ diameter under a pressure of 1 bar. In the experiments, it was found that an ice shell forms close to the droplet surface, at low pressures, this can be seen by the change in droplet shape, and at pressures above 20 bar, this effect appears to be greatly reduced. It is seen that the droplet starts to rotate and turn at the conclusion of combustion. Additionally, tiny jets made of gaseous oxygen that emerge from the surface of the droplet cause the phenomena known as micro explosions. It has also been found that burning constant increases with an increase in pressure [5].

These experimental results from ZARM, combined with their vaporization model motivated this study of numerical modelling of LOX droplet combustion in the hydrogen environment under micro-gravity conditions. This modelling of LOX droplet combustion is intended to simulate the flame and combustion accurately to be coupled with the evaporation model developed by ZARM, which will complete the LOX droplet combustion numerical model. The flame solution can be validated with the experimental results obtained from the drop tower experiments. This work will allow for the study of the fundamental process of LOX/LH_2 combustion and contribute to the optimization of the process.

1.3 Liquid Oxygen Droplet Combustion

The main focus of this study is *LOX* droplet combustion. Figure 1.2 graphically illustrates the physical occurrences associated with droplet combustion. This numerical research is focused on the flame zone and the evaporation of the droplet. Other sub-processes, such as ice formation and micro-explosions are not considered in detail.

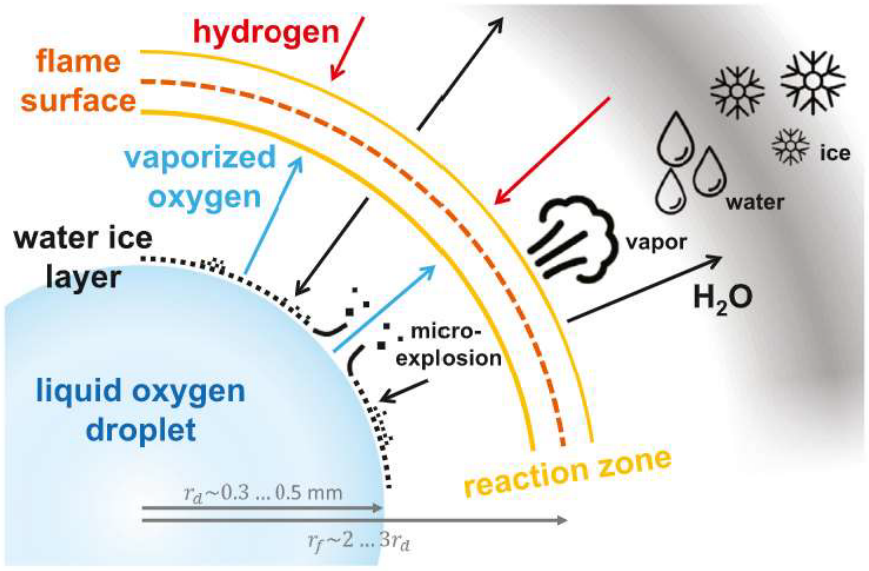

Figure 1.2: Graphical representation of LOX droplet combustion [6]

As seen in Fig. 1.2, initially after ignition, the oxygen from the droplet and hydrogen from the environment react with each other in a radial counter-flow condition and generate a flame zone at a certain stand-off distance from the droplet. This flame zone is at a very high temperature that transfers heat into the droplet in the form of conduction and radiation. Convection is negligible in a micro-gravity environment. The combustion reaction of oxygen and hydrogen generates water (H2O) as the exhaust product around the flame zone. This water vapor condenses and also crystallizes to form ice crystals owing to the cryogenic conditions. This causes micro-explosions on

the droplet, which increases the directional changes as the droplet mass decreases and produces droplet motion as observed in the experimental results of ZARM.

1.4 Goals and Objectives

Now that the motivations and physical processes of the subject of this study are established, this section discusses the overall goals and specific objectives of this study.

1.4.1 Goals

1. To develop an accurate numerical model simulating the flame of LOX droplet in 100% hydrogen.

2. To validate the obtained flame model using experimental data by ZARM.

1.4.2 Objectives

1. Obtain an accurate temperature profile simulating the flame of oxygen and 100% hydrogen that was not achieved in prior studies. This primarily requires a few elements such as:

   (a) Accurate flame temperature

   (b) Accurate stand-off distance from the droplet

   (c) Isothermal temperature profile at the outer boundary

2. Match the rates of heat flow from the newly developed, theoretically accurate flame model with experimental results for similar combustion conditions which will couple both models to give a complete numerical solution.

3. Include radiation heat transfer into the flame model.

Chapter 2

THEORY

This chapter includes a discussion of the physical theory involved in the process under study. The fundamental process behind the combustion of LOX droplets in hydrogen involves the oxidizer (LOX) coming into contact with the fuel (H_2) and then ignition is introduced to start the combustion. The flame in this combustion is a form of diffusion flame. To understand the physical theory behind LOX droplet combustion, it is important to get familiar with the concept of diffusion flames. Concepts discussed in the subsequent theory sections of diffusion flames and droplet combustion are expressed in a detailed way in his personal lecture notes by Dr. Moshe Matalon [12]. The material in this section is derived from this source.

2.1 Diffusion Flames

A diffusion flame is defined as a flame where fuel and oxidizer that are separated initially come into contact with each other in a thin reaction zone with thermal and molecular transport causing combustion and flame front. In this case, molecular diffusion occurs until there is equilibrium and once the equilibrium is reached, the flame stabilizes and maintains shape. A perfect example of a diffusion flame is a candle flame. The vaporized wax is the fuel and it comes into contact with the air which is the oxidizer. The flame is immediately stabilized unless there is a disturbance in the air, which demonstrates the constant molecular diffusion of the fuel and air into the reaction zone.

The rate of diffusion of the reactants into each other is affected by several factors, including the local concentration gradient between the fuel and oxidizer, the temper-

ature of the flame, and the size and shape of the flame. As the reactants mix and react, heat is released, which causes the temperature of the flame to increase, leading to an increase in the rate of diffusion and reaction.

The shape and size of the flame also affect the diffusion process. A flame with a large surface area will allow for more mixing between the reactants, leading to a faster reaction rate. In addition, the shape of the flame can also affect the rate of diffusion. Flames with a wider base have a larger surface area and are more stable, leading to a more efficient diffusion process.

A basic analysis of a diffusion flame can be modeled using a planar steady unstrained diffusion flame by Dr. Matalon [12].

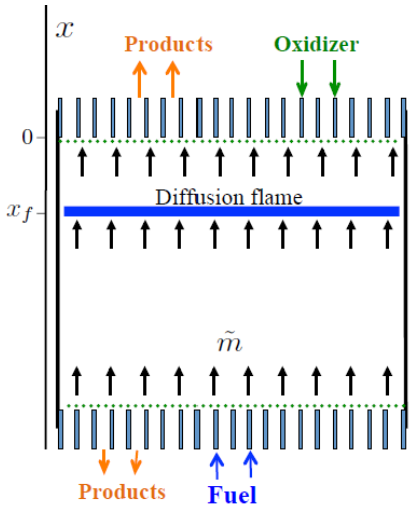

Figure 2.1: Schematic of a planar steady unstrained diffusion flame [12]

As shown in Fig. 2.1, in this case, fuel is supplied in the stream flowing from the bottom of the chamber at a constant speed and the oxidizer diffuses inwards from the top boundary. So there is a flame in the middle of the chamber as shown in Fig. 2.1. With simplified assumptions of unity Lewis number and infinitely fast chemistry, the flame is analytically characterized by the species and temperature profiles as shown

in Fig. 2.2. The analytical solutions of these temperature and species profiles are derived as given in Eq. 2.3 and 2.4.

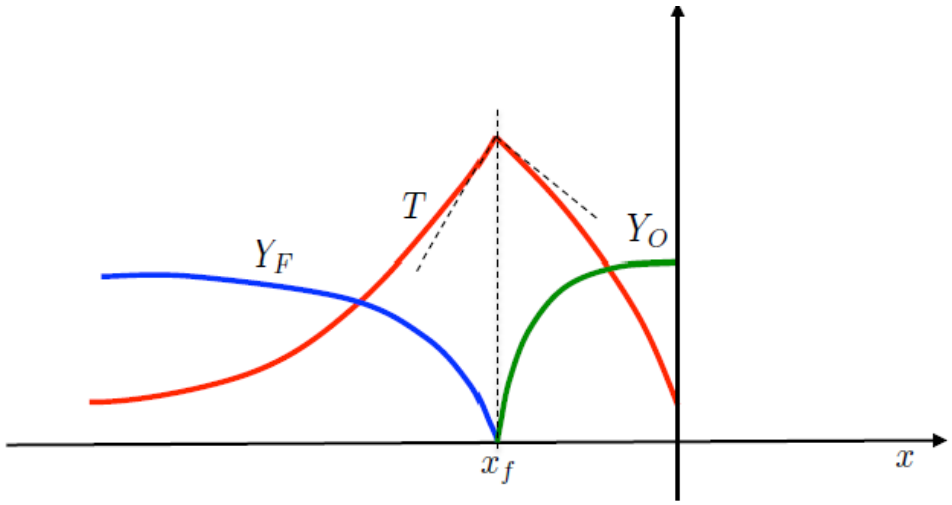

Figure 2.2: Temperature and species profiles of a planar diffusion flame [12]

$$Y_F = \begin{cases} Y_{F0} - (Y_{F0} + \nu^{-1} Y_{O1}) e^{mx} & -\infty < x < x_f, \\ 0 & x_f < x < 0 \end{cases}$$

$$Y_O = \begin{cases} 0 & -\infty < x < x_f, \\ (\nu Y_{F0} + Y_{O1}) e^{mx} - \nu Y_{F0} & x_f < x < 0 \end{cases}$$

Figure 2.3: Species solution of a planar diffusion flame [12]

$$T = \begin{cases} T_0 + \nu^{-1} Y_{O1} e^{mx} & -\infty < x < x_f, \\ T_0 + Y_{F0} - Y_{F0} e^{mx} & x_f < x < 0 \end{cases}$$

Figure 2.4: Temperature solution of a planar diffusion flame [12]

Here, x represents the direction of flow (vertical, as given in Fig. 2.1). The red curve T represents the temperature profile along the domain, Y_O, and Y_F represent the species profiles of oxidizer and fuel respectively and x_f represents the location of flame in the domain.

This general solution for a diffusion flame can be considered as a base or reference for the specialized case of droplet combustion which has the same phenomena occurring in different geometrical and boundary conditions.

2.2 Droplet combustion

The theory of droplet combustion is also explained by using a perfectly spherical fuel droplet with an oxidizer atmosphere surrounding it as seen in Fig. 2.5 [12].

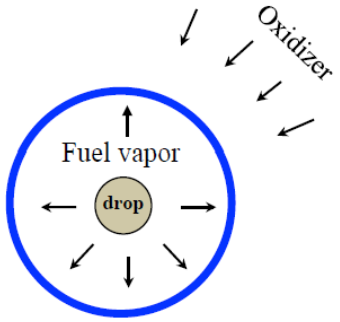

Figure 2.5: Schematic of an ideal droplet combustion [12]

It is similar to the case seen the in the previous section, here instead of the planar flow direction of fuel and oxidizer, the fuel is generally in the form of a spherical droplet from which it evaporates and flows outward. The oxidizer diffuses around the droplet forming a spherical environment where both fuel and oxidizer come into contact. So with an ignition, there is a spherical flame at the point of contact of both reactants. The products then diffuse away from the reaction zone. After defining the

problem, it has been solved using steady-state conservative equations of species and temperature, to find the solution of species and temperature profiles of ideal droplet combustion, as given in Fig. 2.6 and Fig. 2.7.

$$Y_F = \begin{cases} 1 - (1 + \nu^{-1} Y_{O_\infty}) e^{-M/r} & (r < r_f) \\ 0 & (r > r_f) \end{cases}$$

$$Y_O = \begin{cases} 0 & (r < r_f) \\ (\nu + Y_{O_\infty}) e^{-M/r} - \nu & (r > r_f) \end{cases}$$

Figure 2.6: Species solution of a droplet diffusion flame [12]

$$T = \begin{cases} (T_s - L_\mathrm{v})(1 - e^{-M/r}) + (1 + q\nu^{-1} Y_{O_\infty}) e^{-M/r} & (r < r_f) \\ 1 + (T_s - 1 + q - L_\mathrm{v})(1 - e^{-M/r}) & (r > r_f) \end{cases}$$

Figure 2.7: Temperature solution of a droplet diffusion flame [12]

The temperature and species profiles plotted from the derived solution can be seen in Fig. 2.8, similar to the previous solution of planar diffusion flames. As shown in the figure, r refers to the radial distance from the center of the droplet, normalized by the radius of the droplet. The temperature is highest at point r_f, which is the radial location of flame, with respect to the radius of the droplet. It is predictable that the temperature would be maximum at the flame location and reduces either side away from it. It is also noticeable from both solution and the plot, that the species of fuel and oxidizer are completely separated at either end and come into contact at the flame location due to the infinitely fast chemistry being assumed.

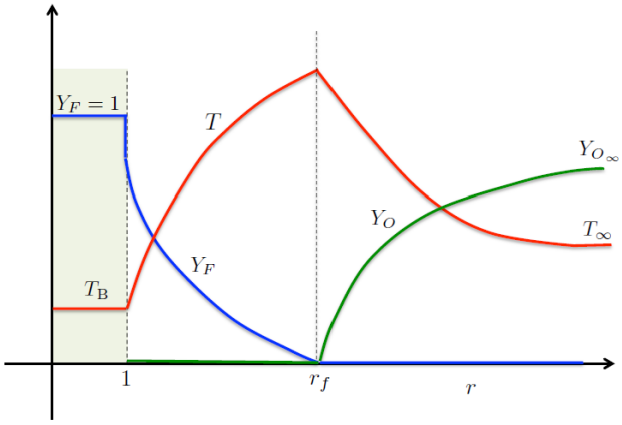

Figure 2.8: Temperature and Species profiles of a droplet diffusion flame [12]

Additionally, the rate of droplet combustion can vary with a few other factors. The size of the droplet can affect the combustion process, with smaller droplets generally having a higher combustion efficiency due to their larger surface-to-volume ratio. In addition, the type of fuel and oxidizer used can also affect the combustion process, with different fuels and oxidizers having different combustion characteristics and flame temperatures.

Chapter 3

NUMERICAL MODELLING AND PROCEDURE

This chapter discusses the entire numerical modelling process followed for this study to simulate the Flame and Combustion of LOX droplet in H_2 under micro-gravity. First, the OpenFOAM software, the governing equations, and the chemistry that are fundamental to the processes learned in the previous section are discussed. These equations that satisfy laws of conservation are solved in the selected OpenFOAM solvers to capture the dynamics of droplet combustion. Then the solvers used in OpenFOAM, the algorithms followed by the solvers, numerical methods used for modelling PDE, and other geometrical and physical conditions specific to this problem are also studied in this chapter.

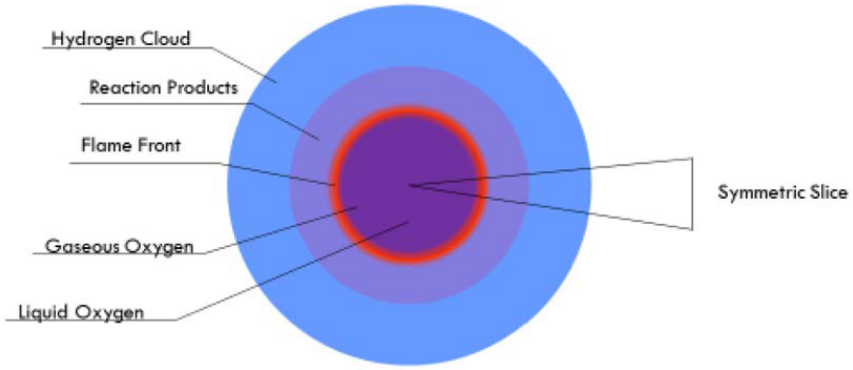

Figure 3.1: Numerically modelled domain of droplet combustion [10]

The spherically symmetric geometry of the problem modeled here is shown in Fig. 3.1. For the purposes of these simulations, the liquid droplet is replaced with an equivalent volume of gaseous oxygen, providing a source of oxygen vapor that

simulates the evaporation rate of the liquid obtained from experimental results. All of the simulations are run in OpenFOAM and the post-processing of results is done in Paraview software of the OpenFOAM library. Additional calculations are done in MATLAB where the heat flow is calculated for the validation of the model. For the simulations, two solvers are used specifically for this study, the reactingFOAM solver of the OpenFOAM which simulates combustion, and the other EBI-DNS solver, which is an independent model developed by a team at Karlsruhe Institute of Technology, Karlsruhe, Germany [20]. The EBI-DNS solver is also programmed to run in OpenFOAM, as it is a variation of the reactingFoam solver itself, with corrections to include better transport and reaction phenomena. The differences in both the models and their equations are clearly discussed in the subsequent sections.

3.1 OpenFOAM

It is important to get familiar with the primary tool being used to simulate the numerical model. OpenFOAM is the simulation software used in this study for all the simulations with both solvers. OpenFOAM, which is short for "Open-source Field Operation and Manipulation" is an open-source and free software developed by OpenCFD Limited. OpenFOAM is a Linux-compatible application written in the C++ programming language. Due to OpenFOAM's strong object orientation, users can add new solvers without altering the primary source code. Users are able to contribute their codes to the OpenFOAM community and aid in growing the constantly growing library thanks to the open-source licensing of OpenFOAM. Users of this software program can use it to solve a variety of differential equations, including those involving lagrangian particle dynamics and finite element analysis (FEA). Due to its extensive library and each solver's individual capacity to solve multi-physics problems, each solver may be used to address a variety of issues and has a particular implementation for the fluid dynamics issue [11]. OpenFOAM is supplied with pre and post-processing environments. The interface to the pre and post-processing are

themselves OpenFOAM utilities, thereby ensuring consistent data handling across all environments [2]. The overall structure of OpenFOAM is given in Fig. 3.2.

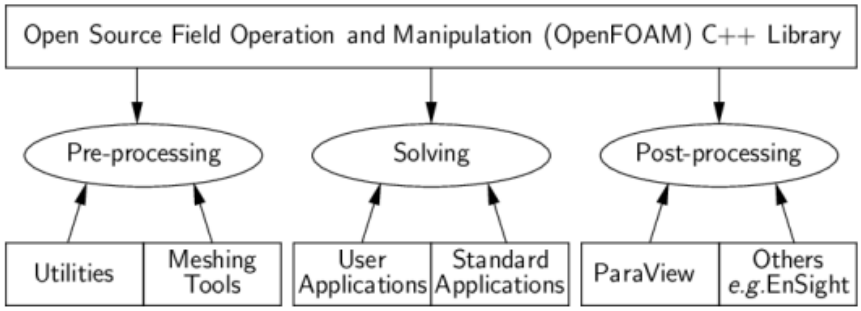

Figure 3.2: General structure of OpenFOAM [2]

The pre-processing utilities of OpenFOAM allow the users to define mesh, initial conditions and boundary conditions that set up the problem. The solver then solves the appropriate partial differential equations by discretizing the domain using various numerical schemes specified in the control file. Then post-processing is finally used to extract results and data from the simulation while also visualizing the domain and results to an extent. Any standard OpenFOAM case file includes 3 folders initially named: '0', 'constant', and 'system'. The '0' folder includes the initial conditions of the simulation, like initial temperature profile, velocities, and species. The 'constant' folder includes the settings or quantities that are constant for the simulation, such as the chemistry of the problem, thermophysical properties, turbulence settings, and any other physical settings. Finally, the 'system' folder of the case is like a cockpit of the simulation which controls the entire simulation. The mesh settings, solver settings, numerical methods, tolerances, and other numerical settings required to drive the simulation are included in this folder.

There are a few advantages and disadvantages of using OpenFOAM to solve this problem of the diffusion flame surrounding an oxygen droplet in hydrogen. The

advantages are: No license fees and Open-source, flexible framework to solve a multitude of problems and extensible for many numerical techniques, advanced modeling capabilities, active user community that provides various inputs and constant support, customizability with source code, portability with various operating systems and platforms. There are also a few disadvantages such as a steep learning curve for new users, limited documentation which can be difficult to understand, limited graphical user interface (GUI) which makes it not very user-friendly, limited technical support as it is an open-source software, and hardware requirements that can be large with high memory requirements. A limitation of existing OpenFOAM software for this specific problem as mentioned previously, is the unity Lewis number assumption in the solvers for simplification, which is unrealistic for hydrogen combustion. Although, for this problem of LOX/LH_2 combustion, a flexible and customizable platform is desirable because of the novelty of the problem. Simplified oxygen and hydrogen are considered with certain assumptions such as a perfectly round droplet, infinitely fast chemistry, uniform pressure in the domain, a quasi-steady process, no turbulence, and no convection.

3.2 Governing Equations

Having obtained an idea of the theory behind droplet combustion, it is now important to establish the concepts required to model the problem at hand numerically. This section defines the governing equations that are required to be solved to model the LOX droplet combustion problem. The governing equations include the ones satisfying conservation of mass, momentum, species, and energy that define any fluid flow and combustion, solved with geometry, initial and boundary conditions pertaining to the LOX droplet combustion in hydrogen. The conservation equations are basically partial differential equations that drive the mentioned quantities within a described domain. These are also the equations that are solved in the OpenFOAM software and EBI-DNS solver with certain approximations/additions.

3.2.1 Conservation of Mass

The governing equation satisfying the conservation of mass can be given by the general continuity equation given in Eq. 3.1. Here, ρ represents the bulk density of the fluid, and $\vec{u}$ represents the velocity vector of the fluid.

$$\partial_t \rho + \vec{\nabla} \cdot (\rho \vec{u}) = 0 \tag{3.1}$$

3.2.2 Conservation of Momentum

The governing equation satisfying the conservation of momentum can be given by Eq. 3.2. Same as the equation in the previous subsection, ρ represents the bulk density of the fluid, and $\vec{u}$ represents the velocity vector of the fluid.

$$\partial_t (\rho \vec{u}) + \vec{\nabla} \cdot (\rho \vec{u} \otimes \vec{u}) = -\vec{\nabla} \cdot P - \vec{\nabla} \cdot \tau \tag{3.2}$$

In Eq. 3.2, The L.H.S terms define the movement of the fluid in all the directions and the R.H.S terms represent the stress forces on the fluid that cause the movement in the given domain. $\vec{\nabla} \cdot P$ refers to the pressure stress forces component and $\vec{\nabla} \cdot \tau$ refers to the viscous stress forces. In this work, the pressure is assumed to be uniform across the computational domain in all the solvers, hence the $\vec{\nabla} \cdot P$ becomes 0. Coming to the viscous stress tensor, considering the fluid as a Newtonian, the deviatoric stress tensor can be given by Eq. 3.3.

$$\vec{\nabla} \cdot \tau = \vec{\nabla} \cdot [\mu(\vec{\nabla}\vec{u} + (\vec{\nabla}\vec{u})^T)] + \vec{\nabla}[\frac{2}{3}\mu(\vec{\nabla} \cdot \vec{u})] \tag{3.3}$$

Where μ is the dynamic viscosity of the fluid. It is determined within the reactingFoam solver of OpenFOAM internally using the Sutherland model which is described in section 3.3.1. The viscosity, μ is not provided as an explicit input in reactingFoam. For EBI-DNS solver it is evaluated using the Chapman-Enskog solution explained in section 3.3.2. The shear stress is considered to be zero, as there is no shear term, so the deviatoric stress tensor should be ideally zero. The movement is given from

the expected Stefan flow phenomenon in the droplet combustion process. It was also observed during the experiments of LOX droplet combustion. that plays a significant role in providing the mass flow conditions in the numerical model.

3.2.3 Conservation of Species

The governing equation satisfying species is particularly applicable for combustion as it involves mass and thermal diffusion. It can be given as Eq. 3.4, where in addition to the previously defined terms for density and velocity, Y_i represents the concentration of all the species involved with i going from 1 to the total number of species. The diffusivity of the species is given by the term D_i, and R_i represents the chemical source term in the reaction.

$$\partial_t(\rho Y_i) + \vec{\nabla} \cdot (\rho Y_i \vec{u}) - \vec{\nabla} \cdot [D_i \vec{\nabla}(\rho Y_i)] = R_i \tag{3.4}$$

While the species are solved during the simulation, the same as density and velocity, the diffusivities D_i and reaction source term R_i are defined and used to solve this equation. But the definitions of these terms can change with respect to the solver. So the differences with respect to this equation in each solver that is being used will be discussed in the next section.

3.2.4 Conservation of Energy

Similar to the species equation, the governing equation satisfying the conservation of energy is also specific to the combustion problem. As the transfer of energy occurs between the flame and the droplet. The governing equation can be written as Eq. 3.5, where all the terms previously defined are still applicable. Additionally, h represents the value of enthalpy, K represents the thermal conductivity, T is the temperature, and $\dot{Q}_{reac}$ is the heat of the reaction.

$$\partial_t(\rho h + \frac{1}{2}\rho|\vec{u}|^2) + \vec{\nabla} \cdot (\rho \vec{u}(h + \frac{1}{2}|\vec{u}|^2)) - \partial_t \rho - \vec{\nabla} \cdot (K \vec{\nabla} T) = \dot{Q}_{reac} \tag{3.5}$$

Same as the species equation, this equation and its terms change based on the solver being used, so it will be discussed in the next section for both the solvers that are used in this study.

3.3 Solvers: reactingFoam and EBI-DNS

As the basic governing equations that are internally solved in OpenFOAM solvers for a combustion problem are discussed in the previous section, this section will now focus on the specific solvers that are used in this study, their assumptions and differences.

3.3.1 reactingFoam

reactingFoam is a solver from the OpenFOAM framework which models various combustion problems with heat and mass transfer. The equations of mass and momentum given in 3.1 and 3.2 will remain the same for this solver. Species and energy, however, are modelled in a slightly different way compared to the given equations. Observing the equation of species given in equation 3.4, the L.H.S consists of a diffusive transport term given by D_i. This diffusion coefficient D_i has to be calculated in either model to solve the given equation. In this case, it is difficult to exactly estimate the molar diffusivities of each species as calculated by the reactingFoam solver. An accurate approximation to evaluate the diffusivities would be a unity Schmidt number assumption as given in Eq. 3.6. This implies that $\nu = D_i$, where ν is the kinematic viscosity.

$$Sc_i = \frac{v}{D_i} \approx 1 \tag{3.6}$$

The Sutherland model which is generally used to calculate the dynamic viscosity of the components in reactingFoam, calculates viscosity based on temperature, using two key parameters: the Sutherland coefficient A_s and the Sutherland Temperature T_s. Additional details on this topic can be found in the OpenFOAM user guide [2]. R_i that is given in the R.H.S of the equation represents the chemical source term,

which can be obtained from reaction rates RR_j and stoichiometric coefficients, $\nu_{j,m}$ of the species as given in Eq. 3.7.

$$R_i = -\sum_{j}^{N_{reac}} \nu_{i,j} RR_j \tag{3.7}$$

In this process of numerical modelling, for the reactingFoam solver, the inputs related to the thermophysical properties are given in the form of Arrhenius coefficients for each species, which are, Arrhenius equation pre-exponential, A_j, temperature exponential of modified Arrhenius equation, β_j and the activation temperature $T_{a,j}$. From these coefficients, the rate factor, k_j of each species can be evaluated as given in Eq. 3.8, which will, in turn, be used to evaluate the necessary reaction rates, RR_j of each species as seen in Eq. 3.9.

$$k_j = A_j T^{\beta_j} e^{\frac{T_{a,j}}{T}} \tag{3.8}$$

$$RR_j = k_j \prod_{m}^{N_{species}} C_m^{\nu_{j,m}} \tag{3.9}$$

Observing the equation of energy given in 3.5, the L.H.S includes a term k that refers to thermal conductivity. It is another such parameter that is difficult to estimate and evaluate how it is being calculated, as it is done internally in the solver. So similar to the previous assumption for diffusivity, conductivity can also be estimated using an assumption of unity Prandtl number, as given in Eq. 3.10, that implies $k = C_p\mu$. The assumptions of unity Schmidt number and Prandtl number indicate the broader assumption of unity Lewis number (which is a ratio of Schmidt number to Prandtl number), indicating approximation of transport and not considering varying transport properties for each species. This assumption is not valid for hydrogen combustion which creates limitations in reactingFoam solver for this study.

$$Pr = \frac{v}{\alpha} \approx 1 \tag{3.10}$$

Similarly, R.H.S of the Eq. 3.5 includes a term $\dot{Q}_{reac}$, which refers to the heat of the reaction, can be defined with respect to the reactingFoam solver as given in Eq.

3.11.

$$\dot{Q}_{reac} = \sum_{j}^{N_{reac}} (RR_j \sum_{m}^{Nspecies} \nu_{j,m} h_{f,m}) \tag{3.11}$$

3.3.2 EBI-DNS

There are certain limitations for the internal reactingFoam solver of OpenFOAM, with regards to our Liquid Oxygen Droplet combustion problem, because of its assumption of unity Lewis number. That is the reason another independently developed solver compatible with OpenFOAM with a variation in reactingFoam solver is used in this study, which is named 'EBI-DNS' solver [20]. The main difference is regarding the species transport, so the equations of species (3.4) and energy (3.5) will be modelled in a slightly different way compared to the reactingFoam solver. The unity Lewis number assumption in reactingFoam indicates that each chemical species in the fluid has the same diffusion coefficient. This assumption may be justified if turbulent transport is more important than molecular transport. But in conditions like this research problem of LOX droplet combustion in hydrogen, where the combustion is laminar because the scales of the domain and molecular transport of each species are highly significant, detailed diffusion coefficients are necessary in order to accurately capture the flame structure.

Therefore in the EBI-DNS solver, the OpenFOAM's general thermophysical classes have been coupled with CANTERA [3], where CANTERA was used as an external library to compute the detailed transport coefficients and chemical reaction rates. Hence a coupled solver has been created where the components of the CANTERA library were made internal to the solver. In the detailed model, the transport of each species is evaluated by taking six gas kinetic properties as input which are: Lennard-Jones collision diameter and energy well depth, polarizability, dipole moment, rotational relaxation collision number, and molecule geometry. These six properties are used to evaluate the binary diffusion coefficients $D_{k,i}$, viscosity μ_k, and thermal

conductivity λ_k for each species k from the Chapman-Enskog solution of the Boltzmann equation as opposed to the Sutherland and other models/equations used in the reactingFoam solver. The mass diffusion coefficient of each species is calculated by applying the Hirschfelder-Curtiss approximation that is given as shown in Eq. 3.12, [17], where X_k is the mole fraction and Y_k is the mass fraction of the k-th species. With every species k having a different mass diffusion coefficient D_k, the molecular mass diffusion flux is also different for each species that is defined as given in Eq. 3.13 [20].

$$\frac{1}{D_k} = \sum_{i \neq k} \frac{X_i}{D_{k,i}} + \frac{X_k}{1 - Y_k} \sum_{i \neq k} \frac{Y_i}{D_{k,i}} \tag{3.12}$$

$$j_k = -\rho D_k \vec{\nabla} Y_k \tag{3.13}$$

These changes in the calculation of thermophysical properties and diffusion coefficients compared to reactingFoam are very crucial. The governing equations for species and energy given in 3.4 and 3.5 respectively are adjusted based on these changes as given in the Eq. 3.14 and 3.15 respectively [20].

$$\partial_t(\rho Y_i) + \vec{\nabla} \cdot (\rho(\vec{u} + \vec{u}_c) Y_i) = R_i - \vec{\nabla} \cdot j_i \tag{3.14}$$

$$\partial_t(\rho h + \frac{1}{2}\rho|\vec{u}|^2) + \vec{\nabla} \cdot (\rho \vec{u}(h + \frac{1}{2}|\vec{u}|^2)) - \partial_t \rho - \vec{\nabla} \cdot (\alpha \vec{\nabla} h) = -\sum_i h_i^o R_i \tag{3.15}$$
$$-\vec{\nabla} \cdot \sum_i h_i((\vec{j_i} + \rho Y_i \vec{u_c}) + \alpha \vec{\nabla} Y_i)$$

Observing the changed species equation, it can be seen that the only difference between the given general equation and the equation of this solver is the correction velocity term $\vec{u}_c$ in L.H.S, which is defined as given in Eq. 3.16. This correction velocity term comes into play because of the varying diffusion coefficients for each species, so it affects the convective term of the species equation as seen [20].

$$\vec{u}_c = \sum_i D_i \vec{\nabla} Y_i \tag{3.16}$$

Similarly, observing the changed energy equation, apart from the slightly readjusted terms, the difference between given general equation and equation of this solver is the last term on R.H.S which redefines the total heat of the reaction $\dot{Q}_{reac}$. It is also a direct consequence of non-unity Lewis number consideration. These are the main differences in the EBI-DNS solver which affect the solution in a huge way that will be seen in the next chapters.

3.4 Equations of State

With the conservation equations being defined in the previous sections, for general OpenFOAM solvers as well as specific solvers for this study, it is important to address one more set of governing equations in this study that is common for all the solvers in general. The closure problem arises in any numerical model because of the terms to be evaluated and the available equation. To solve the closure problem in this model, it is crucial to define the equations of state since they connect the various conservation laws. In this case, the equations of state assume that all the species involved are ideal gases. This assumption works well for gaseous hydrogen under the current simulation conditions, as oxygen moves away from the droplet as it heats up and vaporizes. Although this approximation is also applicable to water vapor near the flame zone, it may not be accurate in the immediate vicinity of the droplet surface for oxygen or near the droplet surface (Approximated gaseous surface in the computational domain)/far-field for water vapor. The OpenFOAM framework's thermophysical modeling library specifies the equation of the state model. To obtain all other properties, the specific heat at constant pressure, Cp, is necessary, and its values for each species are determined from high and low Cp coefficients found in the thermodynamics sub-dictionary of the Thermophysical property data file, sourced from the JANAF thermodynamics table. These coefficients and other thermophysical data are determined using the NIST database [15]. The same kind of coefficients are also given while using the EBI-DNS solver, in the CANTERA file format. So the

equations of state are defined as given in Eq. 3.17, 3.18, and 3.19.

$$P = \bar{\rho} R_u T \tag{3.17}$$

$$\bar{\rho} = \rho \sum_{i}^{N_{species}} \frac{Y_i}{M_i} \tag{3.18}$$

$$h = h_f + \int c_p T \tag{3.19}$$

3.5 Chemistry

As the governing equations are completely defined including the closure problem, the chemistry of the process is introduced in this section, which is a necessary component of the combustion because of the occurence of chemical reactions and formation of new species. In the case of combustion between liquid oxygen and hydrogen, all of the species involved can be given as:

1. H_2: Hydrogen
2. O_2: Oxygen
3. H_2O: Water
4. OH: Hydroxyl radical
5. H: Hydrogen atom
6. O: Oxygen atom

This combustion reaction of LOX/LH_2 can be resolved into a multi-step reaction process. The full mechanism of hydrogen-oxygen combustion is given as a detailed 26-step reaction by Glassman [8]. For simplicity, 1-step, 4-step, and 6-step reaction mechanisms are extracted from this detailed 26-step model. Based on the established

results of previous work [11], the current study used the 6-step reaction for this combustion which uses initiation, propagation, and termination reactions that involve all the mentioned species. The reactions for this 6-step mechanism are presented in Table 3.1, along with their Arrhenius coefficients and reaction rate pre-factors.

Step	Reaction	A	T_a	β
Chain Initiating	$H_2 \implies 2H$	4.52e+19	52530	-1.4
Chain Propagating	$H + O_2 \implies O + OH$	3.55e+15	8353	-0.4
Chain Propagating	$H_2 + O \implies H + OH$	5.08e+04	3166	2.7
Chain Propagating	$H_2 + OH \implies H + H_2O$	2.16e+18	1726	1.5
Chain Terminating	$2O \implies O_2$	6.16e+15	0	-0.5
Chain Terminating	$H + OH \implies H_2O$	3.80e+22	0	-2.0

Table 3.1: Six-step reaction model of oxygen - hydrogen combustion

The six-step chemistry scheme was selected for its ability to provide a reliable estimation of the flame temperature, as well as the heat transferred to the droplet and concentration profiles of the major species. The primary objective of this study is to concentrate on the major species and temperature profiles, rather than minor species concentrations.

3.6 Problem Setup

The pre-processing of a simulation includes setting up the problem in OpenFOAM with all the initial, boundary and meshing conditions. All the simulations in this study for either of the solvers include a similar set of settings and processes before the simulation that will be discussed in this section. First, the computational domain of the problem is created and meshing is done with the software utilities. Later the initial and boundary conditions are saved in the '0' folder of the case file. All the other

physical settings mentioned in the previous section are also entered which concludes the pre-process of the simulation.

3.6.1 Computational domain

With the required domain being the droplet and its hydrogen surrounding, a perfectly spherical droplet is assumed with a perfectly spherical hydrogen environment around it. This assumption works well because of the micro-gravity condition. The overall domain can be seen in Fig. 3.1. For simplification of simulation and reducing numerical complexity, a sector of the spherical domain is considered assuming the droplet and its surroundings to be spherically symmetric. A sector of this domain is thus studied in all the simulations which can be extended to the entire spherical domain. The sector is dissected from the domain with an angle of 5^0 and the curved surface is approximated as a straight planar wall. The domain includes the sector of the droplet and the hydrogen environment around it extending far until 4 cm from the center of the droplet, which is 80 droplet radii away from the center of the droplet. The oxygen is introduced into the computational domain in the gas phase, the vaporization of liquid oxygen at the droplet surface is not modeled directly.

In this study, two computational domains are used differing only in the size of the droplet. One of them to get results from the model and another for the sake of experimental validation. Both of these are formed using the same method described above. The first domain has a droplet diameter of 1 mm, which means that the bounding box of the domain in OpenFOAM starts from the surface of the droplet that has 1 mm as diameter and extends until the 4 cm distance from the center of the droplet. This computational domain can be seen in Fig. 3.3. Similarly, a similar domain with a 700 μm diameter droplet is created as another case in this study. The 1mm droplet diameter case is considered as the baseline for this study, and a few cases of 700 μm diameter droplet cases were solved to validate the model with experimental results.

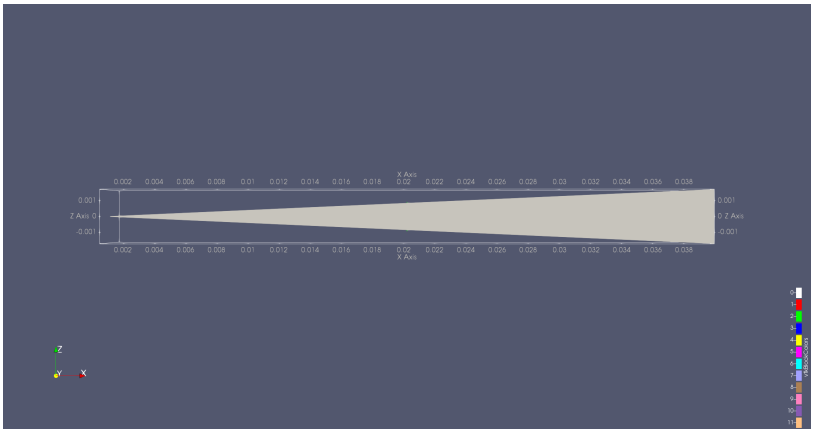

Figure 3.3: Y-axis view of the computational domain of the LOX droplet combustion simulations

3.6.2 Initial and Boundary Conditions

After defining the geometry of the computational domain in the file 'block mesh dict', the initial conditions and boundary conditions can now be implemented using the same geometry labels. The primary initial condition inputs for these solvers are p (Pressure), U (Velocity), and T (Temperature). The initial pressure is always taken to be 1 bar for all the cases, and the initial velocity U is given for the droplet side of the domain, which is the velocity of flow from the droplet. The droplet velocity is calculated using the Stefan velocity phenomenon as given in Eq. 3.20, where k here is the burning rate constant evaluated using experimental results as shown in Eq. 3.21. As shown in Eq. 3.21, k is directly related to the droplet evaporation rate calculated from initial droplet diameter d_0 and droplet lifetime t. The initial velocity is calculated to be 0.43 m/s for the case of a 1 mm droplet and 0.5 m/s for the case of a 700 μm droplet. It is important to note that this blowing velocity calculation is an idealization, as the actual droplets are seen to deform into non-spherical shapes due to the presence of surface ice [4].

$$v_{stefan} = \frac{\rho_{liquid}}{\rho_{vapor}} \frac{k}{8 r_{droplet}} \tag{3.20}$$

$$k_{vap} = \frac{d_0^2}{t}(\frac{mm^2}{s}) \tag{3.21}$$

The temperature initial condition is important to start the combustion reaction, it acts like an ignition for the system. As the spark ignition seemed to have given abnormal results in the previous studies, an assumed initial temperature profile is superimposed in this study, as an initial condition that can start the reaction. The assumed temperature profile is shown in Fig. 3.4, with a peak temperature of about 2500 K. This initial condition for temperature is reported to work well in a previous study [11].

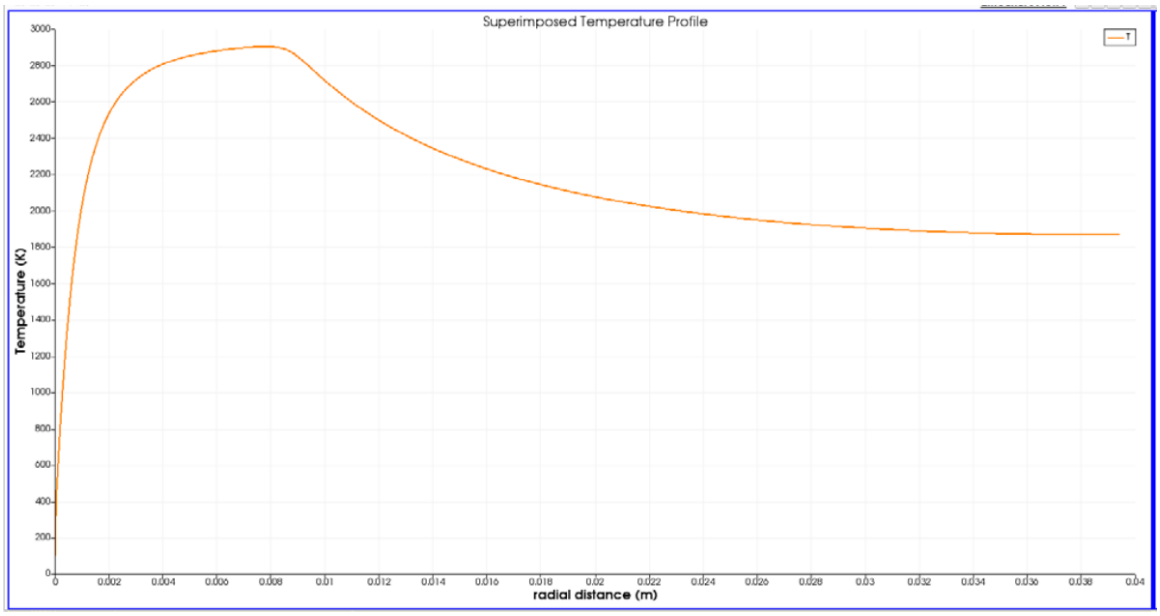

Figure 3.4: Assumed initial temperature profile of the domain [11]

The boundary conditions are applied for each species and also the given quantities of pressure, temperature and velocity. The outer boundary (hydrogen side) is applied an isothermal boundary condition along with outflow, maintaining it at a constant temperature. The inner boundary has a 100% oxygen inlet initially, with a given Stefan flow velocity. The rest of the domain has a 100% hydrogen concentration as

an initial condition. The inner boundary of the domain (droplet surface) also has a boundary condition of 100 K surface temperature.

3.6.3 Constant settings

The constant settings are slightly different in each of the solvers. The reactingFoam solver takes the constant settings similar to all the solvers in the OpenFOAM library, with thermophysical properties, turbulence settings, chemistry settings, reactions, and gravity settings. each of these is presented in different files. The reactions are characterized by Arrhenius coefficients, the viscosity is obtained through the input of Sutherland coefficients, and the thermal characteristics are given by coefficients of specific heats of each species.

The EBI-DNS solver has the same settings but slightly different syntax for each of these inputs. The thermophysical properties in this solver are not taken as an input of Sutherland coefficients for viscosity. As described in section 3.3.2, the properties are given in a single CANTERA input file format of XML, which has the specific heat coefficients and 6 kinetic parameters to evaluate diffusion coefficients. The reactions are also included in the same file as opposed to the reactingFoam solver. The reactions are again similarly characterized using Arrhenius coefficients. In both solvers, a zero-gravity condition is applied because of the micro-gravity environment.

3.6.4 Numerical methods and settings

The numerical controls pertaining to this solver are given into the 'system' folder of each particular case. The controls that are used to run the simulation are given in the 'control dict' file as shown in Fig. 3.5. The simulations are run for a combustion time of 1 second, but the quasi-steady solution is obtained much before this end time. The initial time step is taken to be 10^{-5}, and during the simulation adaptive time step is generally used in OpenFOAM solvers to improve the convergence. But the EBI-DNS solver provides an additional time step control. By default, OpenFOAM can adapt the

time step to the CFL number by setting adjustTimeStep to on and providing a value for maxCo in system/controlDict. In addition, a value for maxFo can be provided in system/controlDict in the EBI-DNS solver. Then, the time step is adjusted according to the CFL number and the Fourier number. The CFL number is computed from $F_o = \frac{a\Delta t}{\Delta x^2}$, where a is the thermal diffusivity and Δt is the simulation time step. The cell size Δx is computed from the cube root of the cell volume. Therefore, this option should only be used in 3D simulations. The maximum fourier number should be below unity, ideally at 0.16. That is maintained as it is for simulations in this study.

The numerical scheme settings used in this study for PDE discretization are given in Fig. 3.6. Time-stepping discretization in OpenFOAM uses an implicit Euler integration which is equivalent to the finite difference method of backward Euler discretization. This gives a certain stability to the solution for complex problems. Apart from time stepping, the gradient and divergence terms are also discretized to model diffusion terms. The grad schemes are discretized using "The Gauss Linear method", while most of the divergence schemes are discretized using the "Gauss limited linear" scheme. The Laplacian term is discretized using the "Gauss linear orthogonal" scheme. In these simulations, the Gauss linear scheme is used where face values are linearly interpolated to neighboring cell centers. This results in a discretization similar to the central differences method found in the finite difference method.

After discretizing the operators, the discretized conservation equations are solved in the solvers using multiple iterative methods. They are generally based on the nature of discretization. Some of these methods include preconditioned conjugate gradient (PCG), preconditioned bi-conjugate gradient (PBiCG), and preconditioned bi-conjugate gradient (PBiCGStab) techniques. The preconditioner involved is a computationally less expensive heuristic that reduces the number of total iterations needed to reach convergence. Preconditioners include diagonal incomplete-Cholesky (DIC) and diagonal incomplete-lower-upper (DILU) methods. The numerical solver settings used for all of the quantities and also the PIMPLE algorithm corrector settings are

given in Fig. 3.7. This is applicable specifically for the EBI-DNS solver, but the general settings for an OpenFOAM solver are also similar with minor changes related to CANTERA in the new solver. With our focus only on the EBI-DNS solver, only the settings related to that solver are shown.

```
application     EBIdnsFoam;
startFrom       latestTime;
startTime       0;
stopAt          endTime;
endTime         1;
deltaT          1e-5;
writeControl    adjustableRunTime;
writeInterval   0.001;
purgeWrite      0;
writeFormat     ascii;
writePrecision  6;
writeCompression off;
timeFormat      general;
timePrecision   6;
runTimeModifiable true;
adjustTimeStep  yes;
maxCo           0.4;
maxFo          0.16;
```

Figure 3.5: Simulation controls in OpenFOAM - EBI-DNS solver

```
ddtSchemes
{
    default         Euler;
}

gradSchemes
{
    default         Gauss linear;
}

divSchemes
{
    default      •  none;

    div(phi,U)      Gauss limitedLinearV 1;
    div(phi,Yi_h)   Gauss limitedLinear 1;
    div(phi,K)      Gauss limitedLinear 1;
    div(phid,p)     Gauss limitedLinear 1;
    div(phi,epsilon) Gauss limitedLinear 1;
    div(phi,k) Gauss limitedLinear 1;
    div((muEff*dev2(T(grad(U))))) Gauss linear;
    div(((rho*nuEff)*dev2(T(grad(U))))) Gauss linear;
    div((thermo:mu*dev2(T(grad(U))))) Gauss linear;
    div(Ji,hsi)    Gauss limitedLinear 1;
    div(phi,Yi_h)  Gauss linear;
}

laplacianSchemes
{
    default         Gauss linear orthogonal;
}

interpolationSchemes
{
    default         linear;
}

snGradSchemes
{
    default         orthogonal;
}

fluxRequired{default yes; p;}
```

Figure 3.6: Solution schemes for partial differential equations in EBI-DNS solver

```
solvers
{
    rho
    {
        solver          PCG;
        preconditioner  DIC;
        tolerance       1e-08;
        relTol          0;
    }

    rhoFinal
    {
        $rho;
        relTol 0;
    }

    p_rgh
    {
        solver           PCG;
        preconditioner   DIC;
        tolerance        1e-09;
        relTol           0;
    }

    p
    {
        solver           PCG;
        preconditioner   DIC;
        tolerance        1e-08;
        relTol           0;
    }

    p_rghFinal
    {
        $p;
        relTol 0;
    }
    pFinal
    {
        $p;
        relTol 0;
    }

    "(U|hs||k|epsilon|Yi|canteraThermo)"
    {
        solver          PBiCGStab;
        preconditioner  DILU;
        tolerance       1e-10;
        relTol          0;
        minIter 1;
    }

    "(U|hs||k|epsilon|canteraThermo)Final"
    {
        $U;
        relTol 0;
    }
}

PIMPLE
{
    momentumPredictor yes;
    nOuterCorrectors  1;
    nCorrectors 6;
    nNonOrthogonalCorrectors 0;

    maxDeltaT       1e-2;
    maxCo           0.5;
    alphaTemp       0.05;
    rDeltaTSmoothingCoeff 1;
    rDeltaTDampingCoeff 1;

}

relaxationFactors
{
    fields
    {
    }
    equations
    {
        ".*"    1;
    }
}
```

Figure 3.7: Solver controls for each solution in EBI-DNS solver

3.7 Meshing

Meshing in OpenFOAM is done using an internal utility called block mesh. The controls of mesh are given in the 'block mesh dict' file, which explains the patch types of each part of the domain and the dimensions of meshing. The sample mesh settings of one of the cases can be seen in Fig. 3.8. It shows the grading of the mesh and where it is more highly concentrated towards the droplet. The mesh grid view of the domain can be seen in Fig. 3.9. The domain consists of around 10,000 mesh cells from inner to outer boundaries.

```
vertices (
    (4.995241107909289E-4 -2.1809693682668E-5 -2.1809693682668E-5)
    (0.0399168 -1.74477548E-3 -1.74477548E-3)
    (0.0399168 1.74477548E-3 -1.74477548E-3)
    (4.995241107909289E-4 2.1809693682668E-5 -2.1809693682668E-5)
    (4.995241107909289E-4 -2.1809693682668E-5 2.1809693682668E-5)
    (0.0399168 -1.74477548E-3 1.74477548E-3)
    (0.0399168 1.74477548E-3 1.74477548E-3)
    (4.995241107909289E-4 2.1809693682668E-5 2.1809693682668E-5)
);
blocks (
    hex (0 1 2 3 4 5 6 7) (200 1 1) simpleGrading (10 1 1)
);
edges ( );
boundary (
  droplet {
    type wall;
    faces ( (0 4 7 3) );
  }
  outlet {
    type wall;
    faces ( (2 6 5 1) );
  }
  top {
    type wedge;
    faces (
      (3 7 6 2)
    );
  }
  bottom {
    type wedge;
    faces (
      (1 5 4 0)
    );
  }
  front {
    type wedge;
    faces (
      (4 5 6 7)
    );
  }
  back {
    type wedge;
    faces (
      (0 3 2 1)
    );
  }
);
mergePatchPairs ( );
```

Figure 3.8: Geometry and mesh controls of an OpenFOAM case

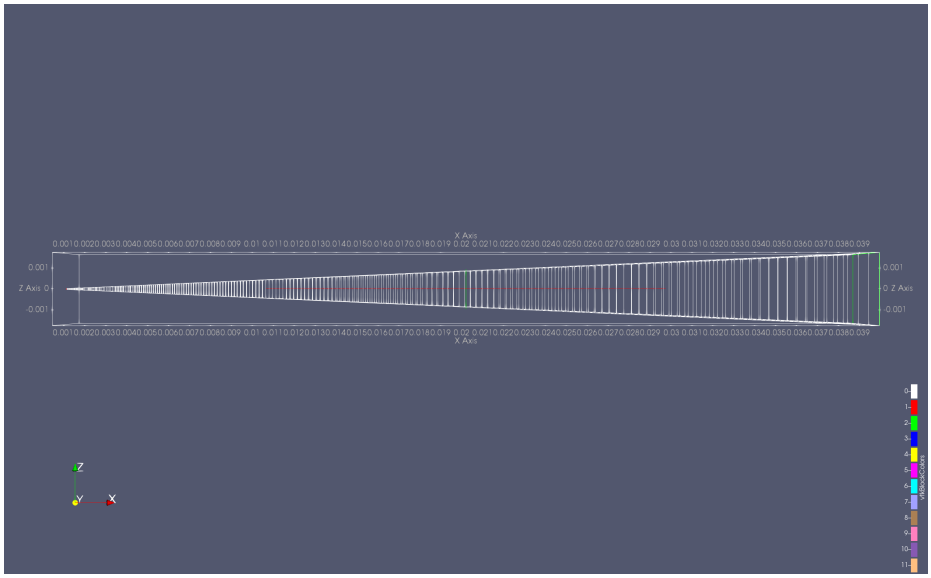

Figure 3.9: Mesh grid view of the domain

3.8 PIMPLE algorithm

The governing equations are solved using the PIMPLE algorithm in both of the solvers in OpenFOAM used in this study. Pressure Implicit with Splitting of Operators (PISO) and Semi-Implicit Method for Pressure Linked Equations (SIMPLE) are the two algorithms that make up the PIMPLE algorithm. The PIMPLE algorithm's flowchart, shown in Fig. 3.10, shows the numerous phases it takes. Once the continuity equation has been resolved, the PIMPLE algorithm is applied. The momentum, species movement, energy, continuity, and equations of continuity provide the foundation of both of the solvers with just differences in equations. More details on how these conservation equations are resolved in the reactingFoam model are given by Doubiani [13]. As shown in Fig. 3.10, species, energy, and velocity are fed into the solver as header files and solved within the chemical loop.

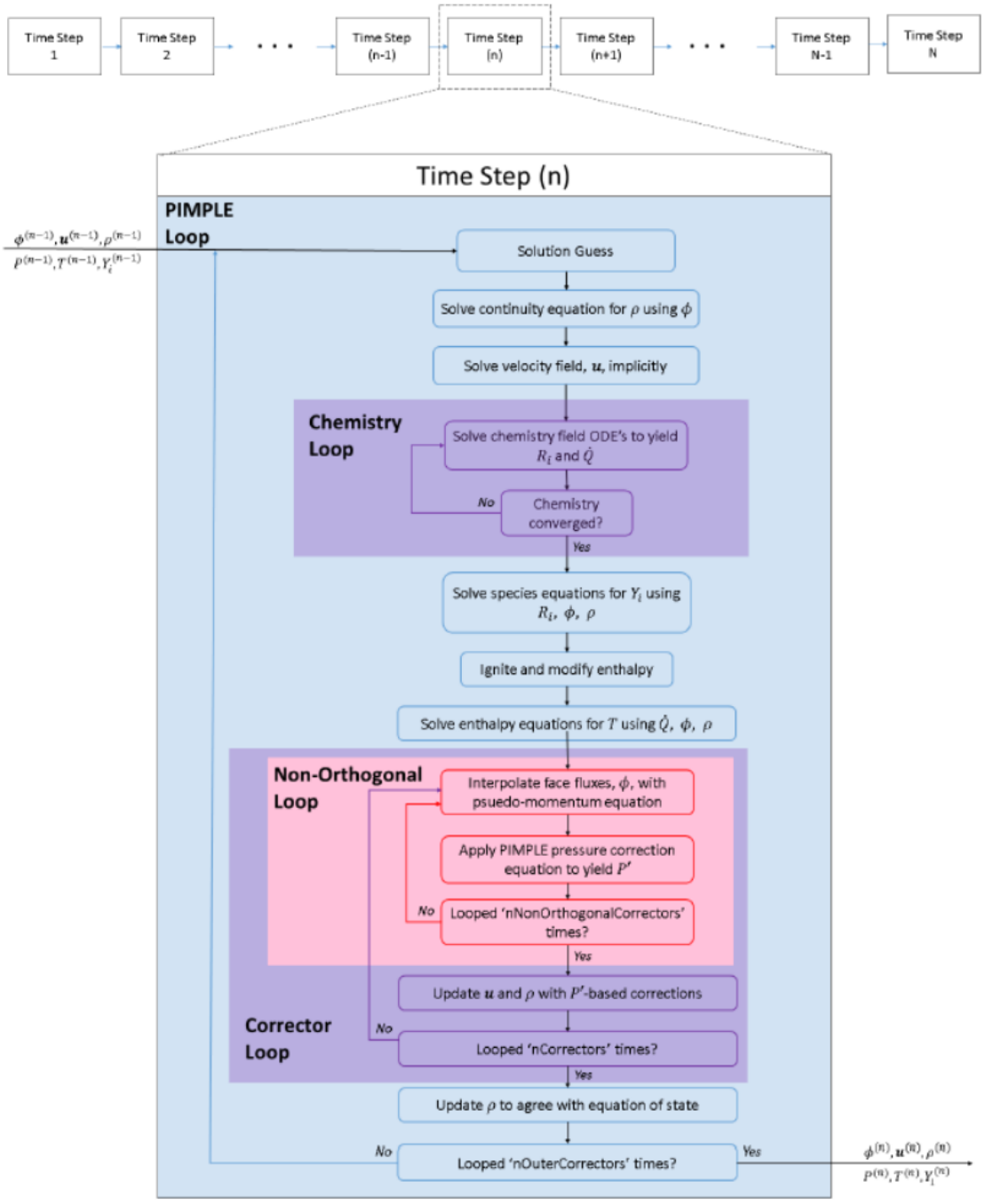

Figure 3.10: Flow chart describing the PIMPLE algorithm [11]

3.9 Post processing

After the simulation is completed the results are viewed and extracted through the OpenFOAM post-processing utility called Paraview. It has a graphical user interface, which allows the users to visualize the domain and results. For this study, the selections are plotted with respect to the spatial coordinate on a center line defined from the x-co-ordinate of the droplet to the x-co-ordinate of the end of the domain. The properties on this line are extracted and studied as results assuming that they are uniform along other directions.

Chapter 4

RESULTS

This chapter discusses the results obtained in this study of LOX droplet combustion in hydrogen. The meaning of the results and validation of the same with experimental results is also discussed, along with possible corrections and reasoning for errors.

4.1 Adiabatic Flame Temperatures

A reference or validation is required to check if the obtained solutions in these simulations are accurate. A simple and primary quantity that is observed in this study to judge the quality of the solution initially is the quasi-steady state adiabatic temperature profile. Specifically, the highest temperature in the temperature profile which is the flame temperature can be compared to the adiabatic flame temperature to check the accuracy of the solution. The adiabatic flame temperature is the theoretically obtained maximum flame temperature for the given conditions and reactants. The adiabatic flame temperatures can be obtained using online tools such as CEARun or CANTERA [3]. For hydrogen-oxygen combustion at 1 bar pressure, with the hydrogen concentrations used in this study, the adiabatic flame temperatures obtained using NASA's CEARUN [18] are given in Table 4.1.

Fuel concentration	Adiabatic (K) (CEARun)	reactingFoam	EBI-DNS
30%H_2 and 70%He	2520	2899	2960
100%H_2	3053	4677	3110

Table 4.1: Adiabatic Flame Temperatures (FT) for various hydrogen concentrations: Adiabatic FT obtained using CEARUN [18], FT obtained in reactingFoam solver, and FT obtained in EBI-DNS solver

4.2 Previous Results

This study is primarily built based on the previous work on this problem done by Gupta [11] and Frydman [9], more prominently Gupta's work on flame modelling with various hydrogen concentrations. Frydman worked on the 1-step and 6-step reaction mechanisms of hydrogen-oxygen combustion with a spark ignition mechanism. In both cases, that work [9] mentions a limitation due to spark ignition which gives very high flame temperatures that are off by about 1500K from the theoretical values. Gupta [11] continued this work by considering an assumed initial temperature profile to start the reaction, instead of a spark ignition, as described in the initial conditions section. That work studied the variation of hydrogen concentrations in the fuel by introducing helium as an inert reactant and also changing the reaction mechanisms from 1-step to 6-steps. That work indicated the accuracy of the 6-step reaction mechanism better than other mechanisms, with flame temperature and temperature profile matching the adiabatic flame temperature for the given concentration of 30% hydrogen and 70% Helium. This can be seen in the temperature profile given in Fig. 4.1.

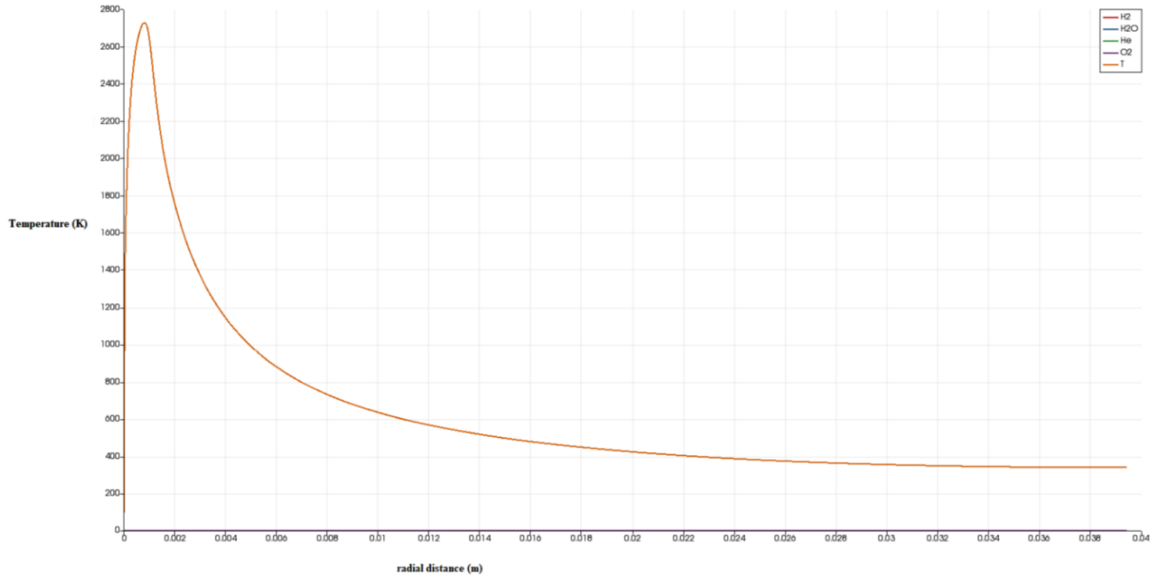

Figure 4.1: Temperature profile of the domain with 30% hydrogen and 70% helium concentration fuel [11].

The flame temperature from the plot of about 2700 K closely matches the adiabatic flame temperature for the 30% hydrogen configuration given table 4.1. With these successful results from this work, these configurations can be set as a baseline to build this current study. Hence this study only focuses on the 6-step chemistry mechanism, as it proved to be more accurate than the 1-step and 4-step from previous work. Coming to the hydrogen concentrations, Gupta's work reported that any concentration higher than 30% was giving vastly inaccurate results with the reactingFoam solver, compared to the adiabatic flame temperatures. The species profiles were also reported to be inaccurate with extremely over-predicted flame temperatures. The current study aims to work on obtaining accurate flame temperature and temperature profiles for a 100% pure hydrogen.

4.3 100% H_2 *case - reactingFoam*

The main goal of this research is to accurately model the combustion flame between O_2 and H_2 that is a part of $LOX$and LH_2 combustion. Ultimately the aim is to obtain an accurate flame model for 100%O_2 and 100%H_2 reactant combustion and explore its connection to the droplet vaporization model. So, using the same conditions of previous work and using the same reactingFoam solver used in previous work, the case of 100%H_2 fuel was simulated initially to dissect the results and understand the reasons for inaccuracy in flame temperature. The temperature profile of this case can be seen in Fig. 4.2, along with the previous result [11] of 30% H_2 using the reactingFoam solver. It can be seen that the temperature profile is very different compared to the previous work. The flame occurs very early in the domain and the indicated flame temperature has an unrealistic value of approximately 4600 K, which exceeds the expected adiabatic temperature by about 1500 K.

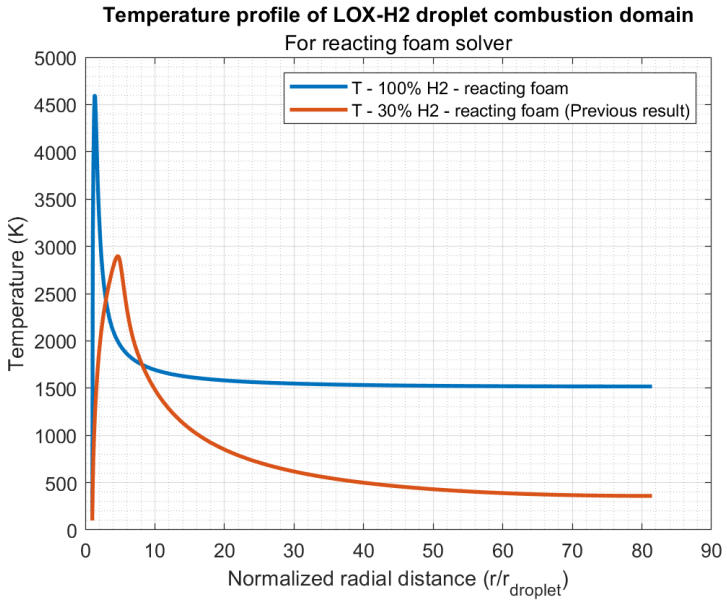

Figure 4.2: Temperature profile of the domain with 100% hydrogen concentration in comparison with 30% hydrogen concentration (previous result) [11], using reactingFoam solver

The clear discrepancy in the results of this case can be primarily attributed to the assumption of unity Lewis number in the reactingFoam solver as discussed in section 3.3.1. As reported in Gupta's work [11], the unity Lewis number assumption results in considering the same diffusion coefficients for all the species which is an approximation. That creates problems with the solution because of the presence of hydrogen in this particular problem, as hydrogen has much higher molecular diffusion characteristics. Molecular diffusion will thus be highly dominant in this combustion specific to species, which will require a consideration of varying diffusion coefficients for each species. This drove the direction of this research towards implementing this correction into the solver or finding a solver or software that includes this correction. Hence, the solver developed by the KIT team named EBI-DNS solver was found through a literature review, which specifically included varying diffusion coefficients into the reactingFoam solver with the same functionality and working, as explained in section 3.3.2.

4.4 EBI-DNS solver results

4.4.1 Counter flow flame

The new EBI-DNS solver is initially configured to solve the standard 2D counter flow flame (CFF) case of the reactingFoam examples in the OpenFOAM library. The reason is to verify the settings and validate the working of this solver, with the existing results of reactingFoam solver for 2D CFF case. The computational domain of the counter flow flame is solved using the new solver for a simulation time of 1 second. A steady state was achieved around 0.22 seconds of simulation time, after which all of the properties including temperature were seen to be constant at any point in the domain. The temperature profile of the solution is shown in Fig 4.3. It can be seen that the temperature profile from the counter flow flame case of reactingFoam can validate this result based on its temperature profile shown in the same figure. This

ensures that the solver is functioning for a similar domain of problems and simulating the problem as it should. The slight difference in the flame can be observed in the species profile of this case given in Fig 4.4. As observed from the reactingFoam species profile given in the same figure, the species transport is higher in the EBI-DNS solver case and a part of the flame is deformed because of this variable diffusion. This also confirms the desirable effect of this solver in the LOX droplet combustion case.

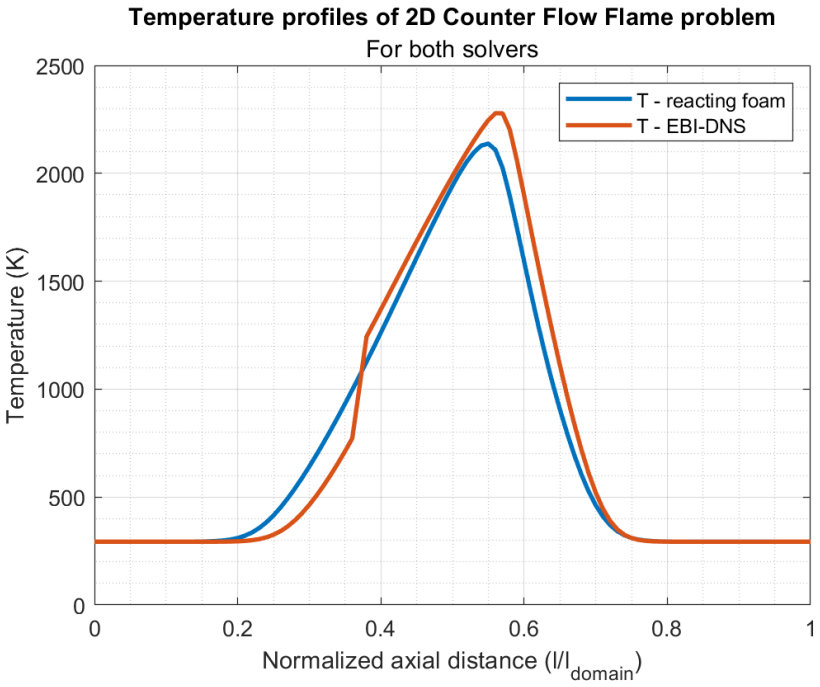

Figure 4.3: Temperature profile of the 2D counter flow flame domain - methane-air reactants

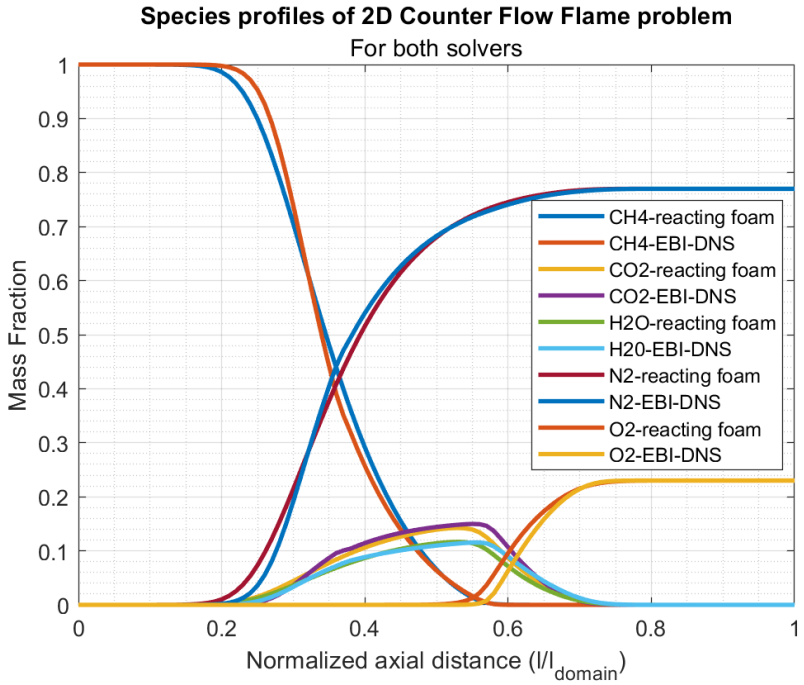

Figure 4.4: Species profiles of the 2D counter flow flame domain - methane-air reactants

4.4.2 LOX droplet flame model - 1 mm droplet

After the solver was verified for the counterflow case, the 1mm droplet diameter case was taken to be the baseline for the $O_2 - H_2$ spherical flame problem. The oxygen droplet of 1 mm diameter considered in the gaseous phase is used for the simulation which is given an initial flow velocity of 0.4 m/s according to the Stefan flow phenomenon calculation obtained from experimental droplet evaporation rate as given in section 3.6.2. The assumed temperature profile shown in the same section is used for ignition and all the other settings are as described in the previous section. This gives the quasi-steady temperature profile of this domain as shown in Fig. 4.5. Comparing this to the reactingFoam case of 100% hydrogen concentration, given in Fig. 4.2, the clear difference in flame temperature and profile can be seen. The flame temperature in this case comes out to be around 3110 K which is much closer to

the adiabatic flame temperature compared to reactingFoam result. This shows that the idea that the unity Lewis number assumption was unreasonable for this reactant combination ($H_2 - O_2$) is plausible and the issue is addressed with the varying diffusion coefficients of the new solver. The species profile of the domain in this case is also observed as shown in Fig. 4.6.

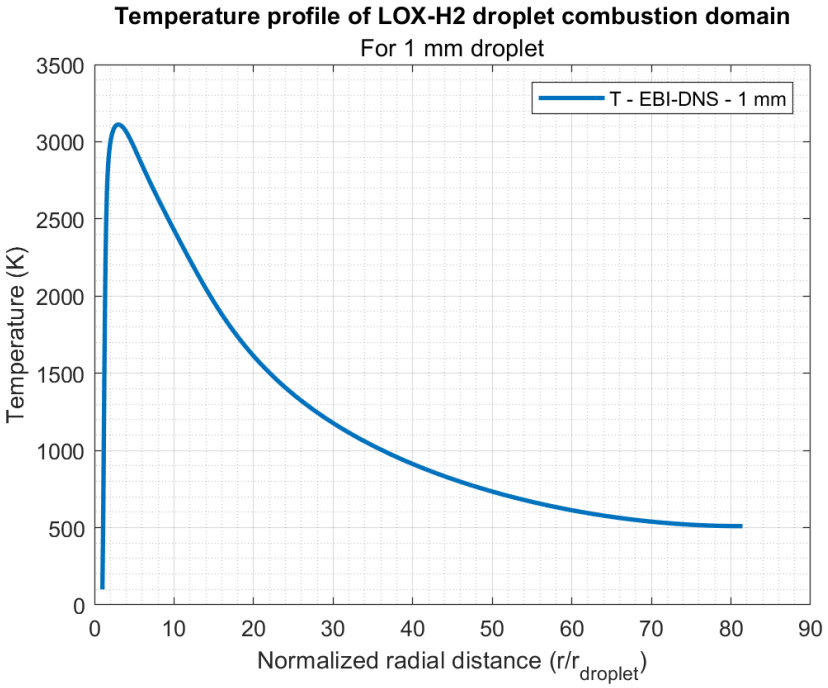

Figure 4.5: Temperature profile of the domain with 100% hydrogen Concentration using EBI-DNS solver

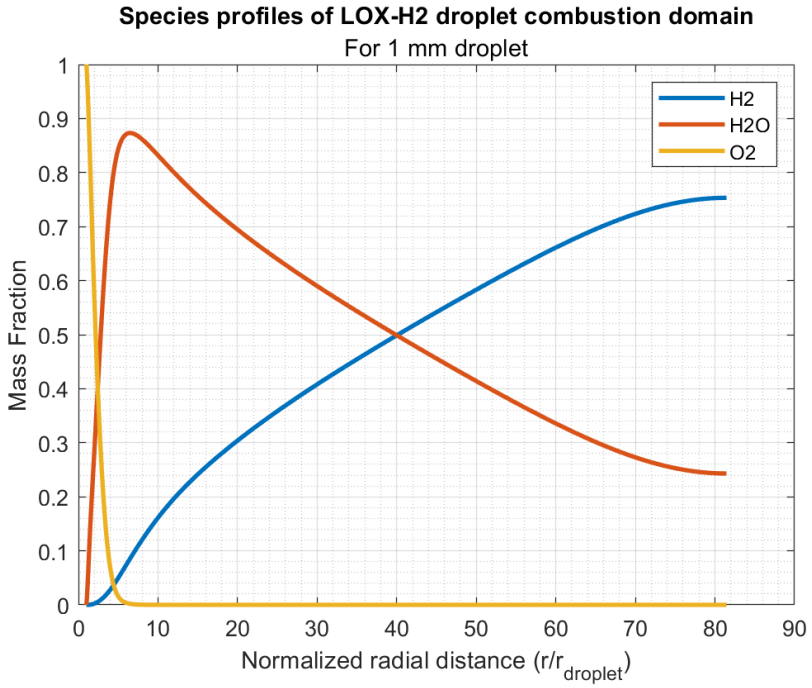

Figure 4.6: Species profiles of the domain with 100% hydrogen Concentration using EBI-DNS solver

4.5 Experimental validation - 700 μm droplet

The baseline result (1 mm droplet) from the previous section shows some success in terms of the reasonableness of the solution, which is discussed in detail in section 4.6. In order for this flame model to be a valid numerical model, it has to be validated with proven data that can be either experimental in general or theoretical estimation. The adiabatic flame temperature is a theoretically obtained value but it only indicates the maximum temperature value. The flame stand-off (f/d) is another reference from experimental data which can be used along with the adiabatic flame temperature to check the validity of the flame solution. Although, as this solution is a numerical model simulating oxygen only in the gaseous phase, the entire solution can be validated with experimental droplet results to obtain a numerically sound solution. One way to do that is to extract the entire numerical profile and calculate the heat

transfer going into the droplet and relate that to the experimentally determined evaporation rate. Currently, heat transfer only through conduction is considered as that is expected to be the dominant heat transfer mechanism in this case of LOX droplet combustion in hydrogen. Radiation is also a significant source of heat transfer, but for the sake of simplicity, it will not be considered in this part of the study. Radiation will be modelled and predicted at later stages to be incorporated into the flame model. Considering the heat transfer going into the droplet through combustion, it can be estimated with the temperature profile as given in Eq. 4.1

$$Q_{flow} = -k_{mix} \times A \times \frac{dT}{dr} \tag{4.1}$$

Where, Q_{flow} refers to the heat flow, A refers to the area of the heat flow (droplet surface), k_{mix} is the effective thermal conductivity of the gas in the vicinity of the droplet, Area is the effective spherical area of the heat flow at the point of calculation, and $\frac{dT}{dr}$ is the gradient of temperature in the domain at any point r. So, based on this result, Q_{flow} calculated at the start of this computational domain, is the heat flow going into the droplet from the flame obtained in this model. If this numerical model is 100% accurate, this value will be exactly equal to the heat rate of vaporization required for the considered liquid droplet in question. Even though practically it cannot be exactly accurate, the degree of matching with this heat rate of vaporization will be useful to judge the apparent fidelity of this flame model. As modelling the actual droplet vaporization is beyond the scope of this study, the heat rate of vaporization for the same conditions as that of the flame model needs to be available, either through experimental results or another numerical model that simulates the droplet and vaporization by itself in similar conditions. The latter option of using a vaporization model developed by the group at ZARM was initially considered as described in Section 4.8. Because of its current working limitations, only the experimental results obtained by the ZARM group [4] from the drop tower experiments are considered in this study.

The experimental results of the 700 μm droplet case are available from the ZARM study [4, 6], where the entire droplet evaporation lifetime in the conditions of 1 bar pressure and micro-gravity, same as the conditions of the model presented here, is given as 136 ms. The heat flow due to evaporation of the droplet from these experiments can be calculated as given in Eq. 4.2. Here, Q_{vap} refers to the heat rate of vaporization of the droplet, $\dot{m}$ refers to the mass flow of the droplet due to evaporation, and h_{vap} refers to the latent heat of vaporization of liquid oxygen, which can be approximately given as 213000 J/kg.

$$Q_{vap} = \dot{m} \times h_{vap} \tag{4.2}$$

The mass flow rate, in this case, can be evaluated using the experimental evaporation rate that can be calculated from the droplet lifetime. The calculation of mass flow rate from droplet lifetime is given in Eq. 3.21 and 4.3, ρ_l is liquid density, and $r_{droplet}$ is the radius of the droplet.

$$\dot{m} = \frac{1}{2} \times k_{vap} \times \pi \times \rho_l \times r_{droplet} \tag{4.3}$$

Using these calculations the experimental value for the heat of vaporization of a 700 μm droplet at 1 bar pressure, is given as shown in Eq. 4.4 to 4.6.

$$k_{vap} = \frac{0.7^2}{0.136} = 3.602(\frac{mm^2}{s}) = 3.602 \times 10^{-6} m^2/s \tag{4.4}$$

$$\dot{m} = 0.5 \times 3.602 \times \pi \times 1204.7 \times 0.0034 = 2.3068 \times 10^{-6} kg/s \tag{4.5}$$

$$\boxed{Q_{vap} = 2.3068 \times 10^{-6} \times 213000 = 0.4938 \text{ Watts}} \tag{4.6}$$

To validate the current numerical model with the experimental result, a case matching the conditions of the experiment needs to be solved. For that purpose, a case of droplet combustion with a droplet of 700μm diameter is constructed, keeping all the other settings exactly the same. That gives results matching quite closely with the 1 mm droplet case with minor changes, showing that the solver results are stable

and reliable. The temperature profile of the case with new droplet size (700 μm) is shown in Fig. 4.7, and the species profile of the same case is given in Fig. 4.8.

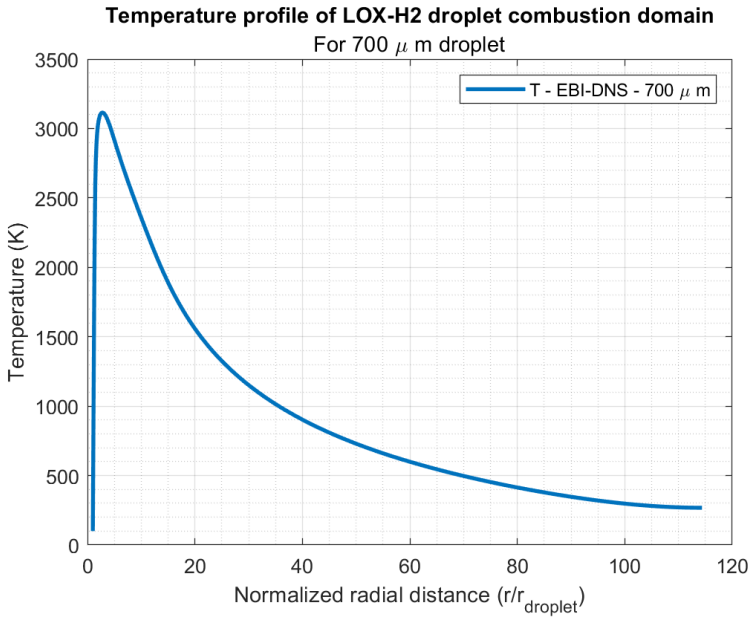

Figure 4.7: Temperature profile of the same case with 700 μm droplet using EBI-DNS solver

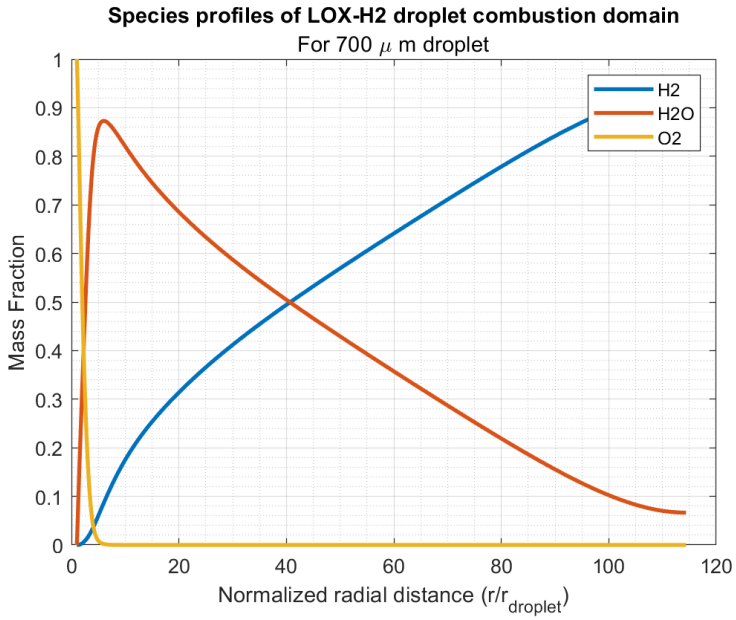

Figure 4.8: Species profiles of the same case with 700 μm droplet using EBI-DNS solver

Having a temperature profile with the same conditions as that of the experiment, the heat transfer through conduction from this flame model to the droplet can be calculated using Fourier's law given in Eq. 4.1. The gradient of the temperature given in the equation is found by fitting a 3rd-degree polynomial to the temperature profile from the droplet surface to the flame. The polynomial fit to the curve can be seen in Fig. 4.9. The gradient is found at the surface of the droplet using the MATLAB function, polyder. The thermal conductivity term k_{mix} given in Eq. 4.1, is the resultant conductivity of the mixture of gases present in the domain. It is estimated using the resultant thermal conductivity equations given in [16]. This calculation gives the conductivity as a function of species mass fraction and temperature. However, at the surface of the droplet, the only species present is 100% oxygen, which can also be verified from the species profile of the solution given in Fig. 4.8. Hence, for simplicity, to calculate the rate of heat transfer going into the droplet, conductivity at

the droplet is considered which is taken as the conductivity of oxygen at the surface temperature of 90K, from the NIST database [15]. That calculation of the expression amounts the value of the rate of heat transfer to be 0.358 Watts as given in Eq. 4.7.

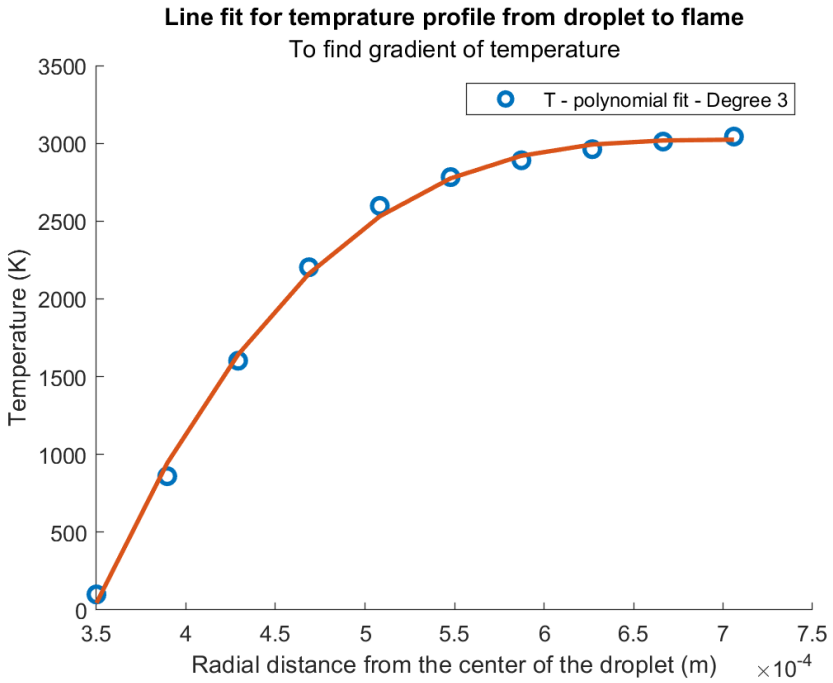

Figure 4.9: Polynomial fit for temperature profile of the 700 μm droplet case using EBI-DNS solver

$$Q_{flow} = -0.0098 \times 1.539 \times 10^{-6} \times 2.5537 \times 10^{7} = \boxed{0.3577 \text{ Watts}} \tag{4.7}$$

4.6 Discussion of results

The EBI-DNS solver results for the 1 mm droplet shown in section 4.4.2, demonstrate a very accurate flame modeling of the LOX droplet combustion in hydrogen (simplified by assuming gaseous oxygen), closer than any of the previous models, with 100% hydrogen. The model flame temperature of 3110.83 K, agrees closely with the adiabatic flame temperature and the species profiles also match the expected results of

the oxygen-hydrogen mixture reaction zone. The flame stand-off distance to droplet diameter ratio (f/d) of this case is found to be approximately 3, which is an accurate stand-off with reference to the experiment, as shown in Fig. 3.1. The simulation is seen to approach a quasi-steady state by around 0.22 seconds of simulation time out of 1 second of simulation time in total, which is significantly slower compared to the reactingFoam solver which achieves a quasi-steady state almost immediately (0.02 seconds). The real time taken for the simulation of 1 second combustion time is also very large (about 15 to 18 hours) compared to the reactingFoam solver (about 4 to 5 hours), which is expected because of the complicated corrections of diffusion coefficients considered in the EBI-DNS solver. The result obtained is verified numerically by considering a grid variation, where the number of grid points was increased to make a finer mesh. It gave similar results demonstrating the grid independence of the numerical model. This showcases the reliability of the solution.

The results of the $700\mu m$ droplet case show the exact same results in terms of temperature profile and species profile, with minor differences because of the size of the droplet. As the size of the droplet is reduced, the flame location is also seen to be changed to around 1.1 mm from the center of the droplet, compared to the 1.5 mm from the center of the droplet from the previous case. Yet, the f/d ratio calculated to be 2.78, still gives a reasonable value that is in agreement with the experiments. The flame temperature of this case also slightly increases to a value of 3114 K, which is not quite significant and is still in close agreement with the adiabatic flame temperature. The experimental validation using this case supports the results of this solver to establish this as a valid numerical model with few shortcomings. The total heat of vaporization in the experiment was found to be around 0.49 Watts, whereas the heat due to conduction from the flame model solution gives the heat going to the droplet only about 0.35 Watts. It appears that the conduction heat transfer alone is insufficient in terms of total heat transferred to the droplet and the difference in the rate of heat transfer can be largely accounted for by including radiation from

the flame to the droplet.

4.7 Correction of the model with radiation

As mentioned in the previous section, the heat deficit in the model can be largely accounted for by radiation. The radiation from the flame to the droplet can be modelled using an assumption of black body radiation. In that case, the total heat transfer can be calculated using the black body emissive power given in Eq. 4.8.

$$E(T) = \sigma T^4 \frac{15}{\pi^4} \int_0^\infty \frac{x^3}{e^x - 1} dx \tag{4.8}$$

$$x = \frac{hc}{kT\lambda} \tag{4.9}$$

The peak wavelength of the flame can be calculated using Wien's law with the flame temperature of 3100 K as about $0.934\mu m$. With this calculation, an assumption that the emissivity of flame exists in the early infra-red region can be made. The radiation heat transfer from the droplet to the surface can be modelled like a thermal circuit, where R_1, R_2, R_{21}, represent the emissivities, or impedances of radiation in basic terms, for droplet surface, flame, and the space in between, given in Eq. 4.12, 4.13, and 4.14 respectively. ϵ_o is the emissivity/absorptivity of droplet surface, ϵ_f is the emissivity of the flame, and F_{21} is the view factor for concentric spheres configuration. The heat transfer for each band of wavelength from x_1 to x_2 can be given as shown in Eq. 4.10.

$$Q_{band} = \frac{\sigma \frac{15}{\pi^4} [\int_0^{x_1} \frac{x^3}{e^x - 1} dx - \int_0^{x_2} \frac{x^3}{e^x - 1} dx]}{R} \tag{4.10}$$

$$R = R_1 + R_{21} + R_2 \tag{4.11}$$

$$R_1 = \frac{1 - \epsilon_o}{\epsilon_o A_1} \tag{4.12}$$

$$R_2 = \frac{1 - \epsilon_f}{\epsilon_f A_2} \tag{4.13}$$

$$R_{21} = \frac{1}{A_2 F_{21}} \tag{4.14}$$

The total heat transferred can be calculated by adding the heat of all the bands in which the emission occurs. For that purpose, the emissivity spectrum of the hydrogen-oxygen flame is required. The lack of precise data on the emissivities of $H_2 - O_2$ flames modeled as black bodies, makes this modelling difficult to reach a reliable solution and out of scope of this study. Based on multiple other studies, a few approaches are proposed in this study to obtain a good radiation model. One is to consider the flame as optically thin and consider the data on spectral emissivities of a similar flame with similar temperatures. Moskalenko *et al.* [14] reported the emissivity of hydrogen-oxygen flames in their study to be around the range of 0.1 to 0.3 in the bands of 4 to 6 μm. But the flame temperature of our study gives the peak wavelength to be much smaller which makes it difficult to interpolate these results. But a fair assumption would be that the emissivities would certainly be very small in the lower wavelengths, hence reducing the total heat transferred compared to the heat transfer calculated using higher wavelengths. The total heat transfer is calculated to be around 0.9 Watts, by considering a wide range of wavelength from $1\mu m$ to $60\mu m$s. This result overpredicts the radiation heat transfer, as the deficit in the model is only about 0.15 Watts. So it can be assumed that the more accurate value of emissivity with calculation in the lower wavelength region, would give a significantly lower heat transferred value which would be more accurate.

Another approach is to consider an optically thick flame region, which would be sensible because of the presence of oxygen and water vapor in the reaction zone. The water vapor is indicated to have certain absorptivity in the range of 0.1 to 0.01 m^{-1} in the infrared region around the predicted peak wavelength [1]. These species can absorb the radiation coming in from the flame making the entire region between the flame and the droplet optically thick. This would result in reduced heat transmission through radiation from the flame to the droplet while still remaining comparable to the conductive heat transfer. This would make the radiation heat transfer compensate for the conductive heat transfer obtained from the numerical model of the flame.

However the radiation amounts to be, the conduction heat transferred obtained by itself is not very far off from the total heat of vaporization experimentally obtained. This radiation modelling can fulfill the small mismatch from both results giving a very good numerical solution.

4.8 Vaporization numerical model

Another numerical model that was considered in this study was a droplet evaporation numerical model developed by the team at ZARM. the initial goal was to match the flame solution obtained from OpenFOAM to the heat of vaporization from this evaporation model as discussed in section 4.5, which would result in a well-rounded numerical solution. It is an independent numerical code written in C++, that is edited using an IDE (Integrated Development Environment) such as CodeBlocks. Following all the equations of conservation and using the same concepts of evaporation mentioned in previous sections, it was developed to simulate the transient evaporation of the droplet considering a surrounding temperature. For this evaporation to agree with the numerical model of flame, the surrounding temperature needs to be around 3000 K. But the limitations that arise in this model are that it only converges for a surrounding temperature of about 110 K and that it has only worked for 700 μm diameter droplet to date. This does not meet the realistic simulation requirements. Hence, the flame model was validated with experimental results instead. Yet, as the OpenFOAM flame model does not directly model the liquid oxygen droplet, a working evaporation model in resonance with the working flame model is necessary to complete the numerical solution, along with radiation.

Chapter 5

CONCLUSIONS

Development of a working numerical model simulating the combustion of LOX droplet in the presence of 100% hydrogen under micro-gravity conditions was successfully carried out in this study. The results show an encouraging model emulating the flame and combustion. Following is the summary of results and takeaways from this study:

- The limitation of unity Lewis number assumption in reactingFoam was overcome with an external solver from literature called "EBI-DNS", which improved the flame model by almost 50%, solely based on flame temperature.

- The solution for the 1mm droplet case, with 1 bar Pressure, is obtained in terms of flame temperature as 3110.83 K, and a flame-stand-off ratio (f/d) of 3, which matches the theoretical and experimental references.

- The solution is replicated for a $700\mu m$ droplet case, with a flame temperature of 3114 K and (f/d) of 2.7.

- The heat transferred from the flame obtained from the flame model to the droplet through conduction is calculated as 0.35 W, which comes close to the total experimental heat of evaporation of the droplet of 0.49 W.

- The small deficit or mismatch in the heat calculated from the flame model and obtained in experiments can be modelled using assuming the radiation heat transfer is non-negligible compared to the conduction.

- The flame region could be considered as optically thick with O_2 and water vapor absorbing the radiation from the flame in the reaction region. The optically thick nature reduces the complete heat transferred through radiation, such that it can be hypothesized that it will be justifying the small difference in heat of vaporization in experiments and the conductive heat transfer.

- The evaporation numerical model developed by Klinkov and ZARM group has limitations. It converges only for surrounding temperatures from 90 K to 110 K. It also only works for a 700 μm diameter droplet. A possible reason could be an error in the calculation of mass fractions of the solution as it breaks down at a certain point in the domain where the mass fraction goes under zero.

Chapter 6

FUTURE WORK

Based on the results and observations in this study, the following are a few of the suggestions for the future prospects of this work:

- Couple the working flame model with a working evaporation model for the same conditions.
- Including an accurate radiation model using either an optically thick/thin assumption of the flame in the infra-red region.
- More data on spectral emissivities of hydrogen-oxygen flame is needed to model the radiation heat transfer accurately.
- Additional data on the absorptivity of the liquid oxygen droplet is also required to complete the radiation model.
- Attempt to optimize the model and solution by reducing computational run time, like using a different chemistry.
- Extending the model to multiple pressure conditions like 2-10 bar, and also different boundary conditions.
- Spark ignition can be reconsidered with the new solver to check if it simplifies the solution.

BIBLIOGRAPHY

[1] *Electromagnetic absorption by water*, wikipedia.org.

[2] Greenshields C.J. *OpenFOAM v10 User Guide*. The OpenFOAM Foundation, London, UK, 2022.

[3] Goodwin D.G., Moffat H.K., Schoegl I., Speth R.L., and Weber B.W. *Cantera: An Object-oriented Software Toolkit for Chemical Kinetics, Thermodynamics, and Transport Processes*. https://www.cantera.org, 2022. Version 2.6.0.

[4] Meyer F. *"Liquid Oxygen Droplet Combustion in Hydrogen under Microgravity Conditions". ZARM*. PhD thesis, December 2022.

[5] Meyer F., Eigenbrod. C., Wagner V., Paa W., Hall J., Zody M., Frydman J., and Hermanson J.C. "Combustion of single oxygen droplets in hydrogen under microgravity conditions". AIAA Scitech, January 2021.

[6] Meyer F., Eigenbrod. C., Wagner V., Paa W., Hermanson J.C., Ando S., and Avila M. "Oxygen droplet combustion in hydrogen under microgravity conditions". *Combustion and Flame*, 241:112081, March 2022.

[7] Williams F.A. *Combustion Theory (2nd ed.)*. CRC Press, 1985.

[8] Glassman I. *Combustion*. Elsevier Science, 1997.

[9] Frydman J. "Transient oxygen droplet combustion in a hydrogen atmosphere: A numerical approach", University of Washington. Master's thesis, June 2018.

[10] Hall J., Zody M., Frydman J., Hermanson J.C., Meyer F., Eigenbrod C., Wagner V., and Paa W. Numerical Simulation of Liquid Oxygen Droplet Combustion in Hydrogen. In *APS Division of Fluid Dynamics Meeting Abstracts*, APS Meeting Abstracts, page C05.003, 2019.

[11] Gupta M. "Numerical investigation of the combustion of liquid oxygen droplets in an environment of hydrogen under microgravity conditions", University of Washington. Master's thesis, June 2021.

[12] Moshe Matalon. *Combustion theory*, lecture series, University of Illinois, Urbana-Champaign, Summer 2013.

[13] Doubiani N. A NOx model tutorial. in proceedings of cfd with opensource software. 2019.

[14] Moskalenko N.I., Zaripov A.V., and Loktev N.F. et al. Emission characteristics of hydrogen-oxygen flames. *J Appl Spectrosc*, 77:378–385, 2010.

[15] Linstrom P.J., Mallard W.G., and Eds. Nist chemistry webbook, nist standard reference database number 69, national institute of standards and technology, gaithersburg md, 20899, 2023.

[16] Bird R.B., Stewart W.E., and Lightfoot E.N. *Transport Phenomena*. Transport Phenomena. Wiley, 2006.

[17] Kee R.J., Coltrin M.E., Glarborg P., and Zhu H. *Molecular Transport*, pages 487–539. John Wiley Sons Ltd, 2003.

[18] Gordon S. and McBride B.J. *"Computer Program for Calculation of Complex Chemical Equilibrium Compositions and Applications"*, 1996.

[19] Heister S.D., Anderson W.E., Pourpoint T.L., and Cassady. R.J. *"Rocket Propulsion"*. Cambridge Aerospace Series. Cambridge University Press, 2019.

[20] Zirwes T., Zhang F., Denev J.A., Habisreuther P., Bockhorn H., and Trimis D. Detailed transport and performance optimization for massively parallel simulations of turbulent combustion with openfoam. In *The 13th OpenFOAM Workshop (OFW13), Shanghai, China, June 24-29, 2018. Ed.: J. Wang*, pages 142–145. CMHL, 2018. 46.11.01; LK 01.

[21] Zirwes T., Zhang F., Hansinger M., Habisreuther P., Pfitzner M., Bockhorn H., and Trimis D. "Quasi-dns dataset of a piloted flame with inhomogeneous inlet conditions". *Flow, Turbulence and Combustion*, 104:997–1027, 2020.